Stellar and wind properties of massive stars in the central parsec of the Galaxy

Fabrice Martins, Reinhard Genzel, D. J. Hillier, Frank Eisenhauer, Thibaut Paumard, S. Gillessen, Thomas Ott, S. Trippe

▶ **To cite this version:**

Fabrice Martins, Reinhard Genzel, D. J. Hillier, Frank Eisenhauer, Thibaut Paumard, et al.. Stellar and wind properties of massive stars in the central parsec of the Galaxy. Astronomy and Astrophysics - A&A, 2007, 468, pp.233-254. 10.1051/0004-6361:20066688 . hal-03784972

HAL Id: hal-03784972
https://hal.science/hal-03784972

Submitted on 30 Sep 2022

HAL is a multi-disciplinary open access archive for the deposit and dissemination of scientific research documents, whether they are published or not. The documents may come from teaching and research institutions in France or abroad, or from public or private research centers.

L'archive ouverte pluridisciplinaire **HAL**, est destinée au dépôt et à la diffusion de documents scientifiques de niveau recherche, publiés ou non, émanant des établissements d'enseignement et de recherche français ou étrangers, des laboratoires publics ou privés.

A&A 468, 233–254 (2007)
DOI: 10.1051/0004-6361:20066688
© ESO 2007

Astronomy & Astrophysics

Stellar and wind properties of massive stars in the central parsec of the Galaxy

F. Martins[1], R. Genzel[1,2], D. J. Hillier[3], F. Eisenhauer[1], T. Paumard[1,4], S. Gillessen[1], T. Ott[1], and S. Trippe[1]

[1] Max-Planck Institüt für extraterrestrische Physik, Postfach-1312, 85741, Garching, Germany
e-mail: martins@mpe.mpg.de
[2] Department of Physics, University of California, Berkeley, CA 94720, USA
[3] Department of Physics and Astronomy, University of Pittsburgh, 3941 O'Hara St., Pittsburgh, PA 15260, USA
[4] LESIA, Observatoire de Paris, 5 Place Jules Janssen, 92195, Meudon, France

Received 3 November 2006 / Accepted 1 March 2007

ABSTRACT

Context. How star formation proceeds in the Galactic Center is a debated question. Addressing this question will help us understand the origin of the cluster of massive stars near the supermassive black hole, and more generally, starburst phenomena in galactic nuclei. In that context, it is crucial to know the properties of young massive stars in the central parsec of the Galaxy.
Aims. The main goal of this study is to derive the stellar and wind properties of the massive stars orbiting the supermassive black hole SgrA* in two counter-rotating disks.
Methods. We use non-LTE atmosphere models including winds and line-blanketing to reproduce *H* and *K* band spectra of these stars obtained with SINFONI on the ESO/VLT.
Results. The GC massive stars appear to be relatively similar to other Galactic stars. The currently known population of massive stars emit a total 6.0×10^{50} s^{-1} (resp. 2.3×10^{49} s^{-1}) H (resp. He I) ionising photons. This is sufficient to produce the observed nebular emission and implies that, in contrast to previous claims, no peculiar stellar evolution is required in the Galactic Center. We find that most of the Ofpe/WN9 stars are less chemically evolved than initially thought. The properties of several WN8 stars are given, as well as two WN/C stars confirmed quantitatively to be stars in transition between the WN and WC phase. We propose the sequence (Ofpe/WN9 $\rightleftharpoons$ LBV) $\rightarrow$ WN8 $\rightarrow$ WN/C for most of the observed GC stars. Quantitative comparison with stellar evolutionary tracks including rotation favour high mass loss rates in the Wolf-Rayet phase in these models. In the OB phase, these tracks nicely reproduce the average properties of bright supergiants in the Galactic Center.

Key words. stars: early-type – stars: Wolf-Rayet – stars: atmospheres – stars: fundamental parameters – stars: winds, outflows – Galaxy: center

1. Introduction

The center of our Galaxy is a unique environment to study massive stars. It harbors three of the most massive clusters of the Galaxy – the Arches, Quintuplet and central clusters. Heavily extinguished and only accessible at infrared (and longer) wavelengths or in X-rays, each of these clusters has a population of more than a hundred massive stars. Even more interesting is the difference in their ages: 2.5, 4 and 6 Myr for the Arches, the Quintuplet and the central cluster respectively (Figer et al. 1999, 2002; Paumard et al. 2006). Such a spread implies the presence of different types of massive objects, naturally sampling stellar evolution in the upper HR diagram. The youth of these clusters, together with their total mass in excess of 10^4 $M_\odot$, partly explains the large number of massive stars in the Galactic Center. But another reason may be the top-heavy mass function: Stolte et al. (2002) for the Arches and Paumard et al. (2006) for the central cluster have shown that the slope Γ of the present-day mass function was shallower than the standard Salpeter value (-0.8 instead of -2.35). This may be due to mass segregation or to a true feature of the *initial* mass function. In that case the Galactic Center could be a peculiar environment for the formation of massive stars.

As a peculiar environment, the central cluster is especially interesting since it harbors the supermassive black hole SgrA*. The first stars ever observed in this region were the so-called "AF" and "IRS16" stars (Forrest et al. 1987; Allen et al. 1990). Their *K*-band spectrum showed strong emission lines – in particular the He I 2.058 μm feature – and they were immediately classified as Ofpe/WN9, a class of evolved massive stars. Further observations by Krabbe et al. (1991) revealed a few additional He I emission line stars. They argued that this population most probably resulted from a burst of star formation a few Myr ago (Krabbe et al. 1995). Detailed spectroscopic analysis with atmosphere models by Najarro et al. (1994, 1997) established that these objects were post-main sequence massive stars. Their UV flux was able to ionise the ISM and produce the nebular Br$_\gamma$ emission, but was far too soft to explain the nebular He I emission. The presence of a population of hotter objects not accessible to observations was thus inferred.

This population was unraveled in recent years. Paumard et al. (2001) found additional stars with broader lines than the initial "He I" stars and typical of Wolf-Rayet stars. Genzel et al. (2003) deduced the presence of even more massive stars from the absence of CO absorption bands. The advent of adaptive-optics assisted integral field spectroscopy lead to a new breakthrough: Paumard et al. (2006) spectroscopically identified nearly a hundred massive stars, including various types of Wolf-Rayet stars, O and B supergiants, and even dwarfs (see also Horrobin et al. 2004; Paumard et al. 2004). Previously, Ghez et al. (2003) and

Article published by EDP Sciences and available at http://www.aanda.org or http://dx.doi.org/10.1051/0004-6361:20066688

Eisenhauer et al. (2005) had shown that the group of stars located in the central arcsecond of the Galaxy and orbiting very close to the black hole (the so-called "S-stars") was composed of early to late B dwarfs.

This latter group of stars is at the heart of an issue usually referred to as the "paradox of youth" of the Galactic center: how could star formation (traced by the presence of young massive stars) have happened so close to the black hole, where the tidal forces should prevent any molecular cloud from collapsing (Morris 1993)? Two scenarios are invoked to solve this problem. In the "in-situ formation" scenario, a disk forms around the supermassive black hole with a density large enough to be self-gravitating so that tidal forces do not perturb the collapse of molecular material (e.g. Levin & Beloborodov 2003; Nayakshin & Cuadra 2005). In the alternate "in-spiraling cluster" scenario, young massive stars are born in a dense cluster several tens of parsec away from SgrA* and its hostile environment, and are subsequently brought to the central region by spiral-in of the parent cluster due to dynamical friction (e.g. Gerhard 2001; Kim & Morris 2003). The former picture (star formation in a self-gravitating disk) appears more attractive since it accounts for a larger number of observational facts (Paumard et al. 2006), but the question is not completely settled.

In that context, it is especially important to get a better knowledge of the physical properties of the massive stars in the central parsec of the Galaxy. In parallel to the development of powerful infrared observational techniques, reliable atmosphere models have become available in recent years. This is due to a huge effort from different groups to include thousands of metallic lines in such models ("line-blanketing"). The use of such models has quantitatively changed our knowledge of the stellar and wind properties of massive stars. To name a few, their effective temperatures are lower (Martins et al. 2002; Crowther et al. 2002; Repolust et al. 2004) and their winds are highly clumped (Hillier et al. 2003; Bouret et al. 2005; Fullerton et al. 2006). In addition to these significant developments, special attention was given to the infrared range. Several studies have been undertaken to compare the parameters derived from IR diagnostics with those obtained from classical optical features (Bohannan & Crowther 1999; Repolust et al. 2005). It appears that the differences are usually small, and certainly within the uncertainties on the derived parameters. Then, both new observational data and better atmosphere models are now available. A quantitative investigation of the stellar and wind properties of massive stars in the central parsec of the Galaxy, in the context of the "paradox of youth", is thus possible.

We present such a study in this paper. Section 2 describes the observational data. In Sect. 3, we present our atmosphere models and explain our method to derive stellar and wind properties. This is followed by a detailed analysis of individual stars (Sect. 4). We then discuss the results with special emphasis on ionising fluxes (Sect. 5), stellar evolution (Sect. 6), metallicity (Sect. 7), stellar winds (Sect. 8) and chemical composition of OB stars (Sect. 9). We finally summarize our findings in Sect. 10.

2. Observations

The observations analysed here were conducted with the integral field spectrograph SPIFFI/SINFONI on the ESO/VLT Yepun 8 m telescope (Eisenhauer et al. 2003a,b; Bonnet et al. 2004) as part of the MPE-Garching GTO program "Galactic Center". A first mosaic of data cubes was obtained on Apr. 8th 2003 using the 250 mas scale in the K band mode, allowing a resolution of ~4000. A second mosaic was observed in $H + K$ band on the same scale on Apr. 9th 2003. These observations were conducted in seeing limited mode since at that time the AO system MACAO was not yet coupled to SPIFFI. A new SINFONI mosaic was obtained on Aug. 18–19th 2004 in K band with the 100 mas scale in adaptive optics mode. Finally, several fields of the region ~15″ north of SgrA* were observed on Mar. 16–17th 2005. Additional information on all these data cubes can be found in Paumard et al. (2006). Two new fields were obtained in the configuration $H + K$/0.1 mas scale on Apr. 20th 2006 and Aug. 16th 2006.

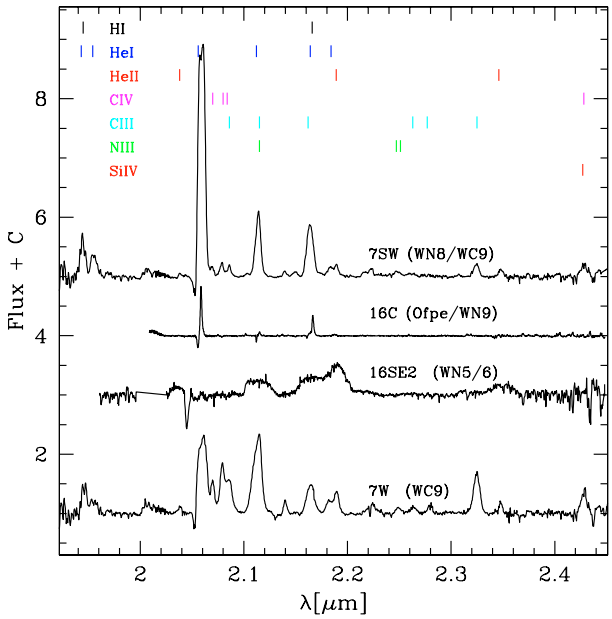

Fig. 1. SINFONI K-band spectra of four post main sequence massive stars observed in the GC. The main lines are marked. Note that all lines are not present simultaneously in one spectrum: depending on the stellar and wind parameters (in particular $T_{\rm eff}$ and abundances), only a subset of the marked lines is observed in a given star.

To extract the spectra out of these cubes, we defined "source" pixels showing spectral signatures of the massive stars identified by Paumard et al. (2006) from which we removed neighboring "continuum" sources to correct for the local background. In the definition of the "continuum" pixels in crowded regions, we paid special attention not to include pixels contaminated by neighboring stellar sources. We used several combinations of source-continuum pixels to check the reliability of the extracted spectrum. We found that as long as contaminating sources are not included, the spectra can safely be extracted. Figure 1 shows typical spectra of various types of stars analysed here together with line identification.

3. Modeling

3.1. Atmosphere models

In order to derive the stellar and wind properties of the massive stars in the central parsec of the Galaxy, we have used state of the art atmosphere models computed with the code CMFGEN (Hillier & Miller 1998). Such models include the main ingredients necessary to produce realistic atmospheric structures and emergent spectra, namely a non-LTE treatment, winds and line-blanketing. The latter has been included only recently since in combination with the two former ingredients it leads to complicated and numerically demanding simulations. But the effects of

line-blanketing are qualitatively and quantitatively very important. Most stellar parameters have to be revised when determined with line-blanketed models due to the strong modification of the radiative transfer caused by additional opacities from metals.

CMFGEN computations proceed in two steps: first the atmospheric structure and radiative field are computed in an iterative process; second, a formal solution of the radiative transfer equation with opacities given by the first step is determined, leading to the detailed emergent spectrum. Details about the code CMFGEN are discussed by Hillier & Miller (1998) and here we only recall the main characteristics:

- *non-LTE treatment*: populations of individual energy levels are computed through the resolution of statistical equilibrium equations including radiative and collisional processes. Non-LTE is especially important for infrared studies since in this range, stimulated radiative processes are greatly enhanced compared to shorter wavelengths (Lenorzer et al. 2004) and thus have a strong impact on level populations.
- *winds*: a spherical geometry is adopted to fully take into account the atmospheric extension due to winds. Velocity gradients in the accelerating wind are also included in the radiative transfer problem. An important point to be noted here is the fact that a velocity law (equivalent to a density law through the equation of mass conservation) has to be adopted since radiative acceleration is not used to compute the hydrostatic structure of the atmosphere. In practice, two approaches are used: for OB stars, a photospheric structure computed with another atmosphere code (usually TLUSTY, see Hubeny & Lanz 1995) is smoothly connected to a so called "β velocity law" ($v = v_\infty(1 - \frac{R_\star}{r})^\beta$) where v_∞ is the terminal velocity and $R_\star$ the stellar radius; for stars with denser winds, the atmosphere is usually optically thick so that the inner velocity structure is less crucial and a law of the form

$$v = v_0 + \frac{(v_\infty - v_0)(1 - \frac{R_\star}{r})^\beta}{1 + \frac{v_0}{v_{\rm core}} e^{\frac{R_\star - r}{h_{\rm eff}}}} \quad (1)$$

  is adopted ($v_{\rm core}$ being the velocity at the bottom of the atmosphere, v_0 the velocity at the expected photospheric velocity and $h_{\rm eff}$ the density scale height of the photosphere). β can in principle be derived from the shape of spectral lines (Puls et al. 1996; Martins et al. 2004) but here, it is only possible in a few cases. Hence, for most of the analysis, we simply adopt the standard value 1.0 (Najarro et al. 1994; Crowther et al. 2006).
  CMFGEN also allows the treatment of non homogeneous atmosphere through the adoption of a clumping law of the form

$$f = f_\infty + (1 - f_\infty) e^{-\frac{v}{v_{\rm init}}} \quad (2)$$

  where f_∞ is the value of f at the top of the atmosphere and $v_{\rm init}$ is the velocity at which clumping appears. We adopted a typical value of $f_\infty = 0.1$ for the remaining stars, unless explicitly indicated.
- *line-blanketing*: CMFGEN includes a direct treatment of metals. The main approximation[1] (which can be easily dropped provided the computational resources are available) is the grouping of levels of similar energies in "super-levels" as initially proposed by Anderson (1991). Through the resolution of the statistical equilibrium equations, level population of metals are computed as for H and He. In the models presented here, C, N, O, Ne, Na, Mg, Al, Si, S, Ar, Ca, Fe, Ni are included for Wolf-Rayet stars and related objects, while C, N, O, Si, S and Fe are used for OB stars. This is due to the lower density winds of the latter which require a better spatial sampling. In that case, minor metals have to be dropped to keep the size of the models reasonable. Note that no super-levels were used for H, He I and He II so that lines from these elements do not suffer from this approximation. In WC stars, we also did not use super-levels for C III and C IV. Finally, we tested the effect of super-levels on the N III 2.247, 2.251 μm lines in WN stars and found it was negligible. In the following, we refer to Grevesse & Sauval (1998) for the solar abundances.
- *temperature structure*: the temperature structure in the atmosphere is set under the condition of radiative equilibrium.
- *microturbulent velocity*: a microturbulent velocity ($v_{\rm turb}$) must be provided in the computation of both the atmospheric structure and the detailed emergent spectrum. In the former part of the simulation, $v_{\rm turb}$ is independent of the position in the atmosphere and we usually choose typical values of 20 km s^{-1} for OB stars and 50 km s^{-1} for Wolf-Rayet stars. For the computation of the detailed emergent spectrum, we adopt $v_{\rm turb} = 10$ km s^{-1}. Note that we have run test models with larger values of $v_{\rm turb}$ for the computation of the emergent spectrum, and found no difference since the lines are mainly shaped by the wind terminal velocity, much larger than $v_{\rm turb}$.

[1] Other approximations concern the treatment of line profiles, redistribution functions and microturbulence.

3.2. Method

The main diagnostics we used for the analysis were: 1) K band photometry and 2) normalized spectra. The number of diagnostics is relatively limited, which sometimes results in degeneracies in the derived parameters, especially when $T_{\rm eff}$ cannot be accurately constrained. The procedure to derive the stellar and wind parameters is as follows:

- *Effective temperature*: we relied on the ratio of lines from successive ionisation states of a given element: He for OB and WN stars, He and C for WN/C and WC stars. In practice, the following lines were used: He I 2.112 μm, He I 2.184 μm, He II 2.037 μm, He II 2.189 μm, He II 2.346 μm, C IV 2.070 μm, C IV 2.079 μm, C IV 2.084 μm, C III 2.325 μm. The He I line at 2.058 μm has been shown to greatly depend on basically *any* parameter (Najarro et al. 1994) and, although it is frequently the strongest observed line, it is not used to derive $T_{\rm eff}$. Unfortunately, two successive ionisation ratios of the same element are not always present, especially for the latest OB and Wolf-Rayet stars. In that case, one usually sees only He I lines so that only an upper limit on $T_{\rm eff}$ can be derived.
  We also define here a temperature $T_\star$ such that

$$L = 4\pi R_\star^2 T_\star^4 = 4\pi R_{2/3}^2 T_{\rm eff}^4 \quad (3)$$

  $R_\star$ is the radius at which the Rosseland optical depth $\tau_{\rm Rosseland}$ is equal to 20 ($R_{2/3}$ corresponding to the radius where the $\tau_{\rm Rosseland} = 2/3$). This definition is useful in the case of evolved massive stars since it is not directly affected by the stellar wind, and since it allows a better comparison of stellar parameters to evolutionary models (see Sect. 7.2).
- *Luminosity*: the main constraint on the luminosity comes from the absolute K magnitude (M_K) which is derived

Table 1. Observational properties of the stars analyzed in this paper. Spectral types are from Paumard et al. (2006). Values of extinction are taken from Schoedel et al. (2007). A distance of 7.62 kpc is adopted (Eisenhauer et al. 2005).

Star	ST	m_K	A_K	M_K	Alternative name
34W	Ofpe/WN9	12.5 ± 0.1	3.0 ± 0.2	–6.0 ± 0.3	GCIRS 34W
16NW	Ofpe/WN9	10.0 ± 0.1	2.3 ± 0.1	–6.7 ± 0.2	GCIRS 16NW
16C	Ofpe/WN9	9.7 ± 0.1	2.3 ± 0.1	–7.0 ± 0.2	GCIRS 16C
33E	Ofpe/WN9	10.1 ± 0.1	2.5 ± 0.1	–6.8 ± 0.2	GCIRS 33E
AF	Ofpe/WN9	10.8 ± 0.1	2.2 ± 0.1	–5.8 ± 0.2	NAME AF STAR
15NE	WN8	11.8 ± 0.1	2.0 ± 0.2	–4.6 ± 0.3	GCIRS15 NE
AFNW	WN8	11.7 ± 0.1	2.3 ± 0.2	–5.0 ± 0.3	NAME AF NW
9W	WN8	12.1 ± 0.1	2.7 ± 0.2	–5.0 ± 0.3	GCIRS 9W
7E2	WN8	12.9 ± 0.1	2.6 ± 0.2	–4.1 ± 0.3	GCIRS 7E2
13E2	WN8	10.8 ± 0.1	2.0 ± 0.3	–6.4 ± 0.4	GCIRS 13E2
7SW	WN8/WC9	12.0 ± 0.1	2.8 ± 0.2	–5.2 ± 0.3	–
15SW	WN8/WC9	12.0 ± 0.1	2.0 ± 0.2	–4.4 ± 0.3	GCIRS 15SW
AFNWNW	WN7	12.6 ± 0.1	2.6 ± 0.2	–4.4 ± 0.3	–
34NW	WN7	12.8 ± 0.1	3.0 ± 0.2	–4.6 ± 0.3	–
16SE2	WN5/6	12.0 ± 0.1	2.6 ± 0.2	–5.0 ± 0.3	GCIRS 16SE2
7W	WC9	13.1 ± 0.1	2.5 ± 0.2	–3.8 ± 0.3	GCIRS 7W
7SE	WC9	13.0 ± 0.1	2.6 ± 0.2	–4.0 ± 0.3	GCIRS 7SE
13E4	WC9	11.7 ± 0.1	2.8 ± 0.3	–5.5 ± 0.4	GCIRS 13E4

from the observed m_K, the distance to the Galactic Center (7.62 kpc according to Eisenhauer et al. 2005), and the extinction taken from the recent work of Schoedel et al. (2007) (see Table 1). Knowing the distance of the sources is a great advantage over many Galactic studies of massive stars. The main source of uncertainty in the luminosity is the extinction which is known to vary in the central parsec. A given value of M_K is obtained for a given flux in the K band which depends on 1) the luminosity and 2) on the wind density. Indeed, free-free emission in the atmosphere can produce an excess of emission mimicking a larger luminosity (Lamers & Cassinelli 1999). Hence, luminosity is derived in combination with wind parameters ($\dot{M}$ and v_∞).

- *Mass loss rate*: $\dot{M}$ is derived from the strength of emission lines formed by recombination. Their intensity depends on the wind density but also on the ionisation of the atmosphere (which is also partly controlled by the density) and on the abundances. The mass loss rate is thus derived in combination with effective temperature and abundances.
- *Terminal velocity*: in stars showing blueshifted absorption profiles and P-Cygni lines, v_∞ was estimated from the velocity shift of the bluest part of the absorption trough with respect to the rest-frame wavelength. For Wolf-Rayet stars with broad emission lines, half of the line width was chosen as typical of the terminal velocity. Values were then refined according to the quality of the fit.
- *Abundances*: the relative H to He abundances can be derived from the intensity of various lines from these elements. As mentioned previously, such a determination cannot be separated from the estimate of $\dot{M}$ and $T_{\rm eff}$ so that a simultaneous determination of these parameters is done. In stars showing C and N lines (C IV 2.070 μm, C IV 2.079 μm, C IV 2.084 μm, C III 2.325 μm, N III 2.247 μm, N III 2.251 μm), constraints on carbon and nitrogen abundances can also be given. Note that we do not use the feature at 2.115 μm for the N abundance determination: it is unclear whether N III is the only contributor (Geballe et al. 2006) and, in addition, the transition oscillator strength is uncertain.
- *Mass*: the determination of masses for hot stars is a challenge. Here, we have used the $M - L$ relation of Heger & Langer (1996) to estimate the present mass of H free Wolf-Rayet stars. For other stars, we did not try to derive masses, the uncertainties being too large.

The uncertainties in the derived parameters are the following: ±3000 K for $T_{\rm eff}$ (±6000 K for the Ofpe/WN9 stars), ±0.2 in $\log \frac{L}{L_\odot}$, 0.2 dex for $\dot{M}$, 30% for the abundances. They are *not* statistical errors (the estimate of such errors would imply the computation of a huge number of models to sample the parameter space around the best fit solution). Instead, they reflect the range of values leading to acceptable fits of the observed spectra. Our errors also do not include any systematic contribution due to uncertainties in atomic data such as collisional and dielectronic recombination cross-sections. This has to be kept in mind when considering the values we quote.

4. Analysis of individual stars

In this section, we give the results of the detailed analysis of individual stars. We mainly focus on Wolf-Rayet and the so-called "He I" stars since their spectra have large enough S/N ratios to allow quantitative spectroscopy. OB supergiants are studied by means of the average spectrum of 10 of them (Paumard et al. 2006). The results are summarized in Table 2. The global methodology presented in Sect. 3.2 is not repeated for each star: we only give specific comments when necessary.

However, as a preamble, we would like to say a few words about the behavior of He I 2.058 μm. It is well known that this line is extremely sensitive to any detail of the modeling, and in particular to the amount of UV radiation. Indeed, the upper level of He I 2.058 μm is directly coupled to the ground state by a transition at 584 Å. Dramatic improvement has been achieved in recent years in the prediction of this UV radiation, mainly due to the inclusion of line-blanketing in the models. However, as we will see in the following analysis, He I 2.058 μm is still poorly reproduced in several stars. Recently, Najarro et al. (2006) have shown that the radiation at 584 Å was partly controlled by the strength of two Fe IV lines: artificially changing the strength of these lines improved the fit of optical singlet HeI lines. We have tried the same kind of tests in the present study, but it turned out that the resulting He I 2.058 μm line profiles were little changed. The reason is partly that in the Wolf-Rayet stars studied here,

He I 2.058 μm is an emission line and is controlled by recombination processes, while in the O stars analysed by Najarro et al. (2006), He I 2.058 μm is in absorption and depends much more on pure radiative transfer effects. Besides, the optical depth of the He I 584 Å line is large in Wolf-Rayet stars, partly controlling the population of the He I 2.058 μm upper level. This does not mean that He I 2.058 μm is not sensitive to the UV continuum: as we will discuss in Sect. 7, subtle blanketing effects can significantly change the appearance of He I 2.058 μm. Having said that, we now turn to the detailed study of individual GC stars.

4.1. Ofpe/WN9 stars

In this section we present the analysis of five Ofpe/WN9 stars. We deliberately exclude the stars IRS16SW and IRS16NE since they are binaries (or candidates, see Martins et al. 2006).

4.1.1. IRS34W

IRS34W is an Ofpe/WN9 star and the faintest of the LBV candidates identified in the Galactic Center (Paumard et al. 2004). Trippe et al. (2006) also showed that it had recently experienced photometric variability attributed to the formation of dust in material possibly ejected in a LBV-like outburst.

Due to the absence of a strong $T_{\rm eff}$ indicator, we could find several solutions to the fit of the K band spectrum by varying the He content, the luminosity, and the mass loss rate for $T_{\rm eff}$ in the range ~20 000–~33 000 K. Figure 2 shows one of the possible best fit models. For the acceptable effective temperatures, the He/H ratio is larger than solar, in the range 0.25–0.6, while the mass loss rate goes from 6×10^{-6}–2×10^{-5} $M_\odot$ yr^{-1} and the luminosity is found in between 3 and 6×10^5 $L_\odot$. It is important to note that these parameters are not independent and only certain combinations within these ranges are acceptable. For example, low $T_{\rm eff}$ imply low luminosities, large $\dot{M}$ and large He/H ratio.

The morphology of Br$_\gamma$ is well sampled in our observed spectrum. In particular, the blue side of the Br$_\gamma$ emission line shows a "shoulder" and, at even shorter wavelengths, a small absorption dip. This results from the combination of two effects: first, Br$_\gamma$ is a P-Cygni profile for which the blue absorption dip is partially filled by emission; second, several He lines with both emission and absorption profiles add to this Br$_\gamma$ shape. The contribution of each element is shown in the insert in Fig. 2. The exact shape of this complex profile depends on the wind density in the line formation region, and consequently depends on both β and the filling factor f (in addition to the mass loss rate and the He/H ratio). In order to fit this profile, we had to choose β in the range 2.0–4.0, i.e. larger than 1, the value commonly found in O supergiants. This is due to the fact that larger β leads to narrower profiles with stronger absorption dips and emission peaks (see Martins et al. 2004). Similarly, the best fits were obtained with *unclumped* models. This is at odds with the current knowledge that winds of massive stars are strongly inhomogeneous. However, since this complex line profile depends on several parameters, we refrain from concluding that the wind of IRS34W (and the other similar Ofpe/WN9 stars) are homogeneous. More detailed investigations with high resolution spectroscopy should help to better resolve this line and improve our determination.

The only feature not well reproduced by our models is the emission at 2.112–2.115 μm: it is wider in the observed spectrum than in our models. The main reason is that this emission is a blend of several lines, the identification of which is still under debate. The concensus is that both He I 2.112 μm (blue part, through P-Cygni profiles) and N III 2.115 μm (red part) contribute to the emission. Clearly, the He I emission is present in our models but we are not able to reproduce the N III emission. Actually, we are not convinced that this emission is really due to N III since we do not detect the lines N III 2.247 μm and N III 2.251 μm. Geballe et al. (2006) recently claimed that O III could be responsible for that emission. Since the oscillator strength for this transition is very uncertain, we decided not to fit the red part of the emission complex at 2.112–2.115 μm.

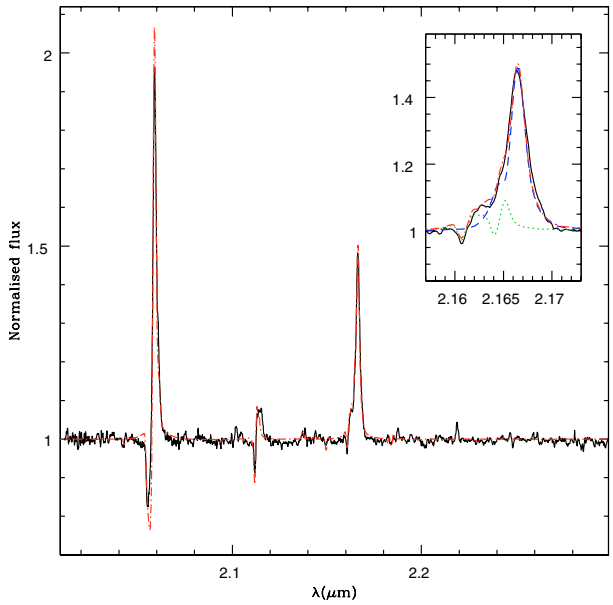

Fig. 2. Best fit (red dot-dashed line) of the observed K band spectrum of IRS34W (Ofpe/WN9, black solid line). The insert is a zoom on the Br$_\gamma$ line, showing the contribution of H (blue dashed line) and He I (green dotted line) to the total synthetic profile (red dot-dashed line).

4.1.2. IRS16NW

The spectrum of IRS16NW is similar to IRS34W with the exception that the emission part of the 2.112 μm complex is weaker and the He lines on the blue wing of Br$_\gamma$ are mainly in absorption. However, IRS16NW is 2.5 mag brighter, leading to a higher luminosity. The best fit model of its K band spectrum is shown in Fig. 3. For this star too, the only problem is the emission at 2.112 μm which is absent in our model. As for IRS34W, large β and unclumped models gave the best fits.

Compared to the analysis of Najarro et al. (1997), we find a larger $T_{\rm eff}$, although the range of values for which a fit can be achieved encompasses their value. The luminosity is lower by a factor 2.4, while $\dot{M}$ is lower by a factor of 4.7. We also find a terminal velocity smaller by 150 km s^{-1}. The main difference with Najarro et al. (1997) is the He content that we find larger than solar but smaller than the H content. In our case, this indicates that IRS16NW has probably only recently left the main sequence and is in an early evolved status.

4.1.3. IRS16C

IRS16C is the brightest star of our sample. It is one of the Ofpe/WN9 stars first discovered in the GC. As for the other stars of the same spectral type, its $T_{\rm eff}$ is poorly constrained. Figure 4 shows one of the best fit models. A large value of β as well as an unclumped wind are favoured as for IRS34W. The feature at

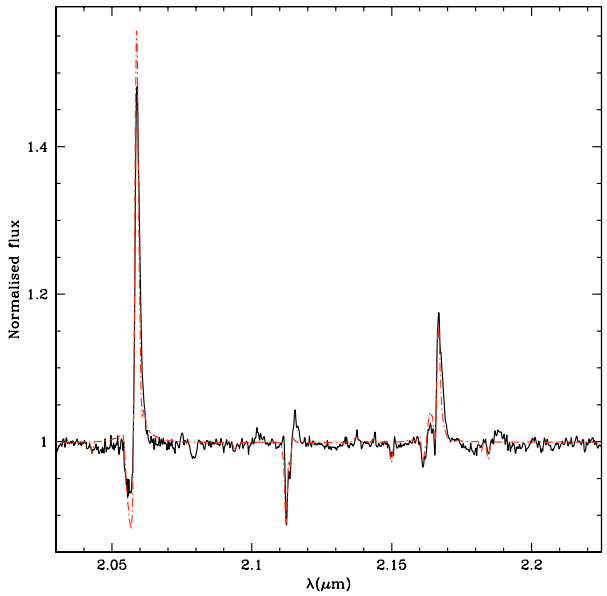

Fig. 3. Best fit (red dot-dashed line) of the observed K band spectrum of IRS16NW (Ofpe/WN9, black solid line).

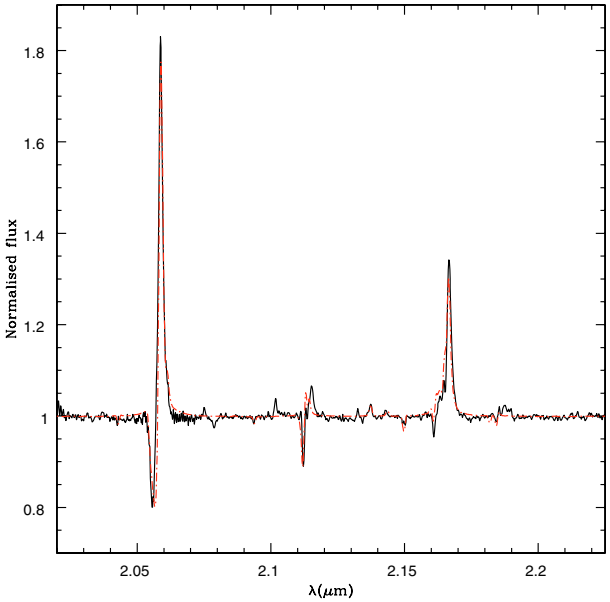

Fig. 4. Best fit (red dot-dashed line) of the observed K band spectrum of IRS16C (Ofpe/WN9, black solid line).

2.115 μm is not reproduced in our model, as well as the one at 2.100 μm. These lines could be from N III, but the absence of N III 2.247 μm and N III 2.251 μm emission weakens this possibility. We detect a Mg II emission at 2.138 μm. This emission is reproduced by our model for a twice solar Mg content. However, this value should be interpreted with care given the uncertainty in $T_{\rm eff}$ and the weakness of the line.

As for IRS16NW, we find a lower He content and a lower mass loss rate compared to the results of Najarro et al. (1997).

4.1.4. IRS33E

The spectrum of IRS33E is similar to IRS34W, IRS16NW and IRS16C, and so are the derived properties. The best fit model is shown in Fig. 5. As for IRS16C, the weak emission lines

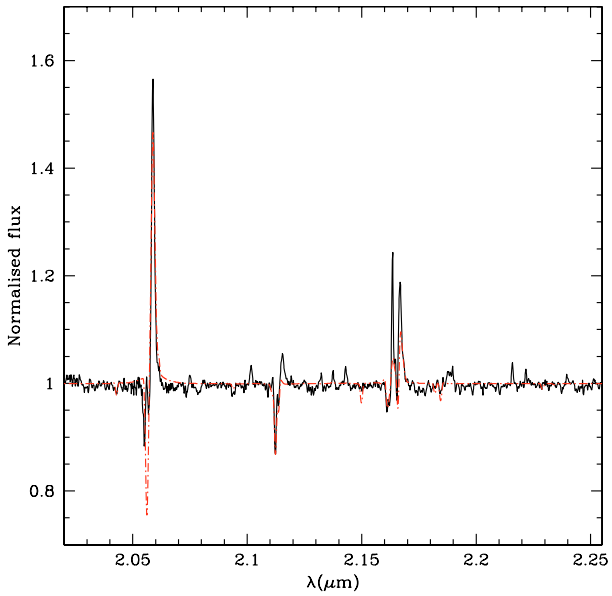

Fig. 5. Best fit (red dot-dashed line) of the observed K band spectrum of IRS33E (Ofpe/WN9, black solid line).

at 2.100 μm and 2.115 μm are not reproduced. Note that the structure of the Br$_\gamma$ emission is real and is observed at different epochs.

4.1.5. AF star

The AF star is one of the first GC stars discovered and analysed. Based on its SINFONI K band spectrum, Forrest et al. (1987), Allen et al. (1990) and Najarro et al. (1994) classified it as a Ofpe/WN9 star. However, compared to the other stars of the same type presented above, AF has much broader lines. This indicates a stronger wind and possibly a more advanced evolutionary state (see also Sect. 6.2). The best fit to the $H + K$ band spectrum is shown in Fig. 6. The effective temperature is poorly constrained due to the absence of He II lines, as for the other Ofpe/WN9 stars. This implies a degeneracy between $T_{\rm eff}$ and He/H: models with 18 000 K $\lesssim T_{\rm eff} \lesssim$ 30 000 K and 0.5 $\lesssim$ He/H $\lesssim$ 5.0 gave reasonable fits (lower He/H being required at larger $T_{\rm eff}$). Such behavior was already noted by Najarro et al. (1994). We also found that $\dot{M} \sim 10^{-4}\ M_\odot\ {\rm yr}^{-1}$ were necessary to fit emission at low $T_{\rm eff}$, while values of the order $1.5 \times 10^{-4}\ M_\odot\ {\rm yr}^{-1}$ were sufficient at high $T_{\rm eff}$. The luminosity is in the range $1{-}2 \times 10^5\ L_\odot$. The values derived by Najarro et al. (1994) are consistent with our cool/He-rich/large $\dot{M}$ models. The analysis of this star illustrates perfectly the degeneracy one has to face when $T_{\rm eff}$ is poorly constrained. In contrast to the other Ofpe/WN9 stars analysed before, the shape of the Br$_\gamma$ complex is dominated by the wind, so that the contribution of the He lines blueward of Br$_\gamma$ is not resolved. Hence, the He content is poorly constrained. In the comparison to the Najarro et al. (1994) results, it is also important to note that a different extinction was used. We adopted $A_K = 2.2$ while Najarro et al. had $A_K = 3.0$. This influences the results, in particular the luminosity and the mass loss rates (through their influence on M_K, see Sect. 3.2).

4.2. WN stars

In the following, we present the results of the detailed study of 5 WN8, 3 WN7, 1 WN5/6 and 2 WN8/WC9 stars. For all the

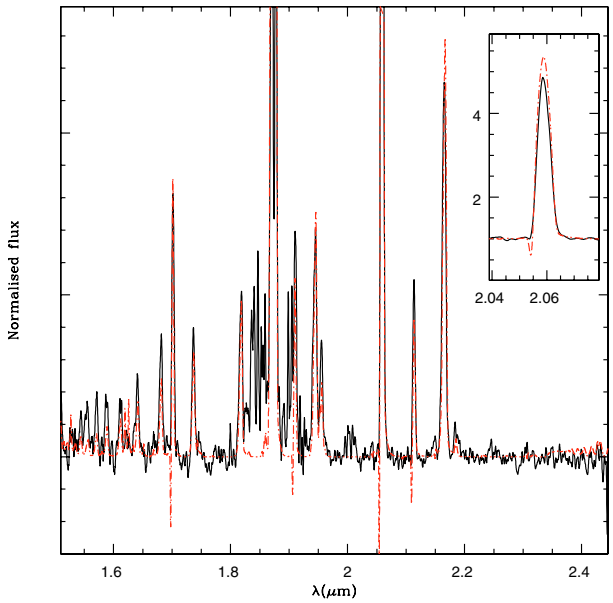

Fig. 6. Possible fit (red dot-dashed line) of the observed $H + K$ band spectrum of the AF star (Ofpe/WN9, black solid line). Other combinations of $T_{\rm eff}$, He/H and $\dot{M}$ lead to similar fits. The observed spectrum around 1.85 μm is noisy and should be disregarded. See text for discussion.

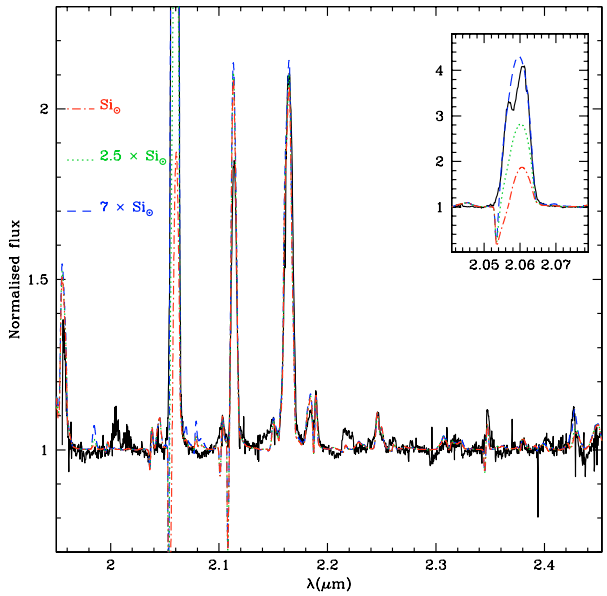

Fig. 7. Best fit (red dot-dashed line) of the observed K band spectrum of IRS15NE (WN8, black solid line). The different broken lines indicates models with similar parameters except the Si content. When it increases, the fits of Si IV 2.427 μm and He I 2.058 μm are improved. See text for discussion.

WN8 stars, the H content is relatively low, but we cannot discriminate between H free stars and stars with X(H) of a few percent. We thus quote a H mass fraction $\lesssim$0.1.

4.2.1. IRS15NE

Figure 7 shows our best fit spectrum of the WN8 star IRS15NE. The He II lines at 2.037, 2.189 and 2.346 μm are well reproduced and allow a good estimate of the effective temperature. The fit of the N III 2.247, 2.251 μm features is good, providing an accurate N abundance determination. The main discrepancy concerns the He I 2.058 μm line which is too weak. Reducing $T_{\rm eff}$ improves the fit but weakens the He II lines. The Si IV feature at 2.427 μm is also slightly too weak if a solar abundance is used for Si. Figure 7 shows the effect of increasing the Si content by a factor of 2.5 and 7. Interestingly, the fit of the SiIV line improves, as well as the fit of He I 2.058 μm! However, several weak Si lines appear around 1.98 and 2.08 μm. We do not detect these lines. Hence, we cannot safely conclude that a super-solar Si abundance is required for IRS15NE. The problem of Si IV 2.427 μm in the initial model may be due to incorrect atomic data for this line. In terms of atmospheric structure, changing the Si content translates into a slight variation of the temperature structure (T is reduced in the outer atmosphere) which is then responsible for the strengthening of He I 2.058 μm (see also Sect. 7.2). This highlights once more the extreme sensitivity of He I 2.058 μm to the very details of the modeling.

IRS15NE was previously studied by Najarro et al. (1997) who found a lower $T_{\rm eff}$, a larger luminosity and a larger mass loss rate. The terminal velocity and He content were similar to the present value.

4.2.2. AFNW

AFNW is located North West of the AF star and was assigned a spectral type WN8 by Paumard et al. (2006). The presence of

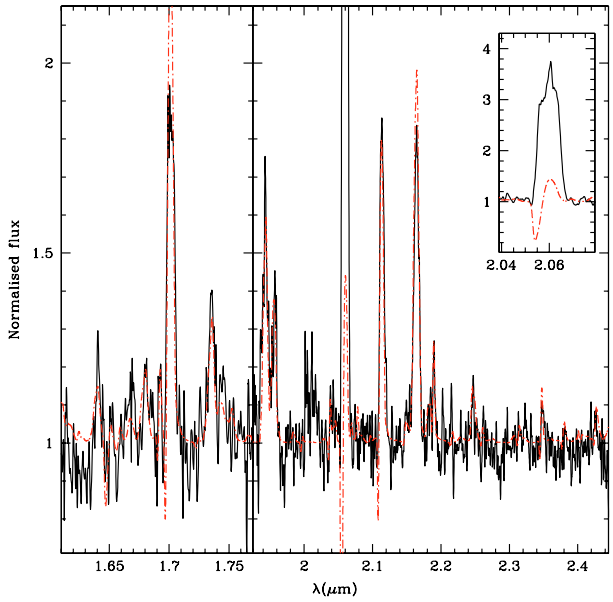

Fig. 8. Best fit (red dot-dashed line) of the observed H band (*left*) and K band (*right*) spectrum of AFNW (WN8).

both He I and He II lines allows a rather robust $T_{\rm eff}$ determination (see Fig. 8). Only He I 2.058 μm is too weak and He I 1.700 μm too strong in our model.

4.2.3. IRS9W

IRS9W is the WN8 star of our sample with the cleanest spectrum and the strongest He II lines. Figure 9 shows that our best model is able to perfectly reproduce most of the features, with the notable exception of He I 2.058 μm. Given the quality of the observed spectrum and the presence of several HeI and He II lines very well reproduced by our model, we think the effective temperature is well constrained (see in particular the

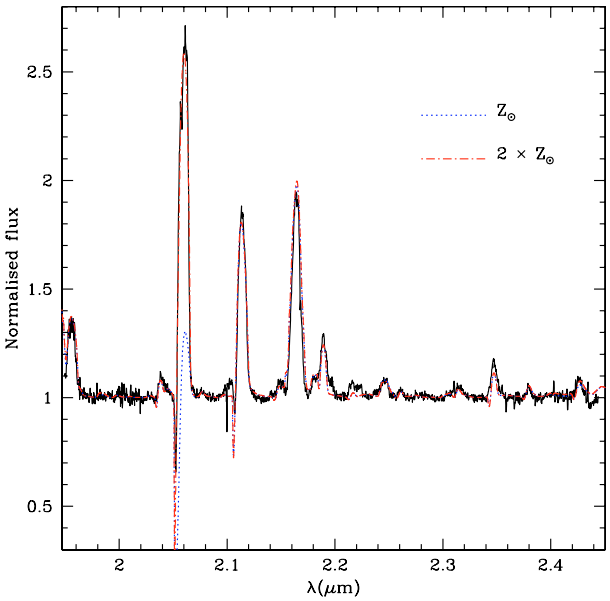

Fig. 9. Best fit of the observed K band spectrum of IRS9W (WN8, black solid line). The blue dotted line is a model with $Z = Z_\odot$ while the red dot-dashed line is for $Z = 2 \times Z_\odot$. Note the change of He I 2.058 μm with metallicity, tracing its extreme sensitivity to UV radiation.

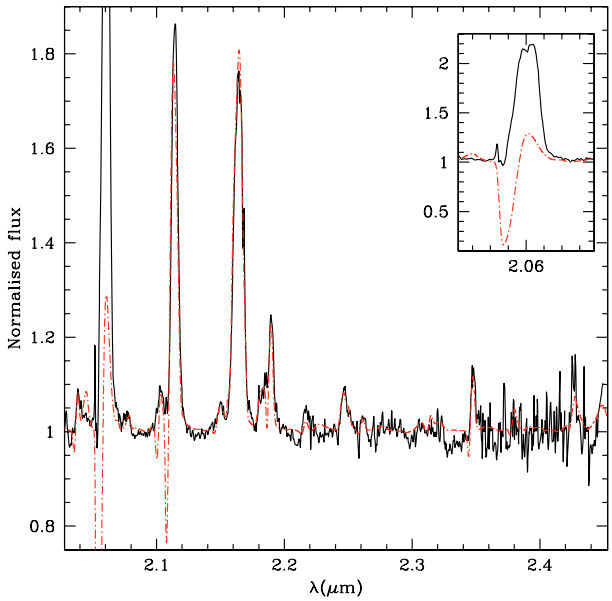

Fig. 10. Best fit (red dot-dashed line) of the observed K band spectrum of IRS7E2 (WN8, black solid line).

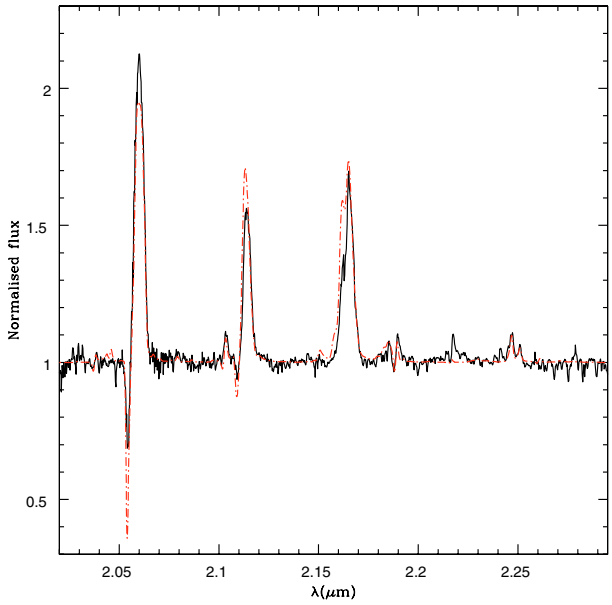

Fig. 11. Best fit (red dot-dashed line) to the observed K band spectrum of IRS13E2 (WN8, black solid line).

ratio of He II 2.189 μm to He I 2.184 μm). Decreasing $T_{\rm eff}$ to strengthen He I 2.058 μm leads to weaker He II 2.037, 2.189 and 2.346 μm lines. Modifying the luminosity and mass loss rate so that they still lead to a good match of the observed K band magnitude and of the strength of emission lines does not lead to any improvement as far as He I 2.058 μm is concerned. Interestingly, the situation got better when we tried to increase the global metallicity to a value of 2 times $Z_\odot$. In that case, we could get a strong He I 2.058 μm line without degrading the fit of the other diagnostics. This points once again to the extreme sensitivity of He I 2.058 μm to UV opacities, a larger metallicity corresponding to a softer UV radiation. A more detailed discussion of the behavior of He I 2.058 μm as regards metallicity changes is given in Sect. 7.2.

4.2.4. IRS7E2

The best fit model to the K band spectrum of IRS7E2 is shown in Fig. 10. All lines are well reproduced, except He I 2.058 μm. The excellent fit of the N III 2.247, 2.251 μm line allows a good N abundance determination. $T_{\rm eff}$ is also well constrained since He II 2.189 μm, He II 2.037 μm and He II 2.346 μm are clearly detected. As for IRS9W, we have tried to increase the metallicity to improve the fit of He I 2.058 μm, but this time, the line barely reacted and remained too weak.

4.2.5. IRS13E2

IRS13E2 is the brightest member of the IRS13E cluster and is classified as WN8. Our best fit model is shown in Fig. 11. An effective temperature of 29 000 K was required to fit the He spectrum. It is the most luminous WN8 star of our sample However, the presence of dust in the IRS13E cluster may hamper our determination. We will argue in Sects. 4.3 and 6.5 that we probably derive only an upper limit on the luminosity.

Najarro et al. (1997) already mentioned the stars of IRS13E in their study, but at that time they could not resolve the components and analysed the global spectrum. Hence, a direct comparison with their results is meaningless.

4.2.6. IRS7SW

Paumard et al. (2006) classified IRS7SW as WN8, but in view of the present results (see below), we refine its identification to WN8/WC9. Our best fit model is presented in Fig. 12. The preferred $T_{\rm eff}$ allows a reasonable fit of the Carbon lines and of He II 2.189 μm, but seems a little too low to account for He II 2.037 μm and He II 2.346 μm. However, increasing $T_{\rm eff}$ leads to a too strong He II 2.189 μm line. The presence of C IV and C III as well as N III lines indicates that IRS7SW is likely a WN/WC star. This is confirmed by the abundance determination (see also Sect. 6.3 for a quantitative discussion). We

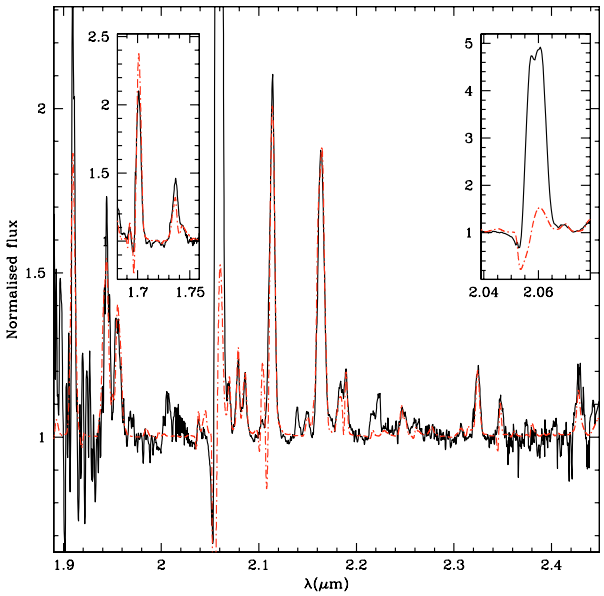

Fig. 12. Best fit to the observed $H + K$ band spectrum of IRS7SW (WN8/WC9).

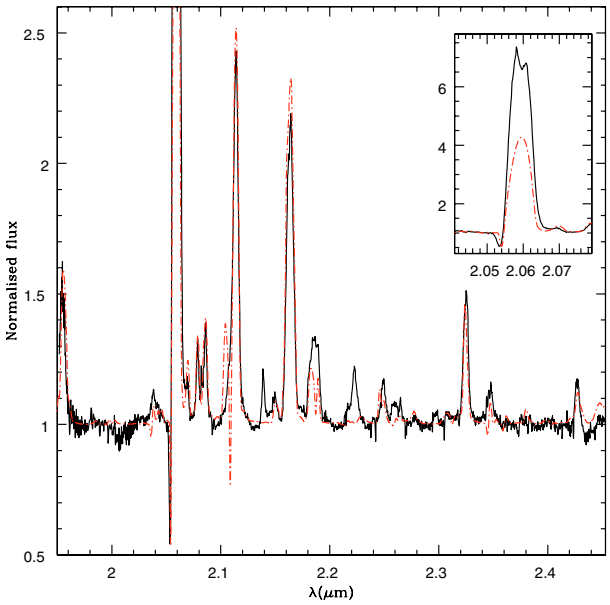

Fig. 13. Best fit (red dot-dashed line) to the observed K band spectrum of IRS15SW (WN8/WC9, black solid line).

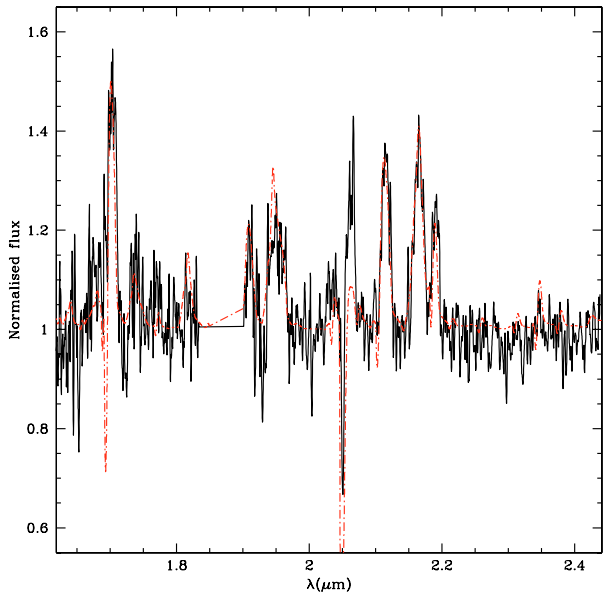

Fig. 14. Best fit (red dot-dashed line) to the observed $H + K$ band spectrum of AFNWNW (WN7, black solid line). The region around P_α was cut since it is not reliable. The observed spectrum was also smoothed for clarity.

also note two unidentified lines: one feature at 2.140 μm, and another one at 2.224 μm. The former cannot be attributed to Mg II 2.138 μm since $T_{\rm eff}$ is too high. Besides, Mg II 2.138 μm is a doublet while we clearly see only one component. The line at 2.224 μm cannot be due to Na I since again $T_{\rm eff}$ is too large. Interestingly, these lines are also found in most of the WC9 stars of our sample, as well as in the WN8/WC9 star IRS15SW (see next section). We conclude that they are typical of C-rich stars. Note that these lines are also present and not identified in the WC9 stars of the Figer et al. (1997) sample (see their Fig. 9).

4.2.7. IRS15SW

IRS15SW is a late WN star showing C lines in its K band spectrum so that it was classified as WN8/WC9 by Paumard et al. (2006). Most of the lines are reproduced by our best model (Fig. 13). A notable exception is the He I/He II complex around 2.185 μm. The emission is stronger than our model. Changing $T_{\rm eff}$ does not help since we fit either the blue or red side of the emission but never the whole complex. Besides, $T_{\rm eff}$ is relatively well constrained by the other He II lines. We also do not perfectly fit the blue absorption dip of He I 2.058 μm. This may require a larger v_∞, but in that case the other emission lines are too broad. The C lines are perfectly matched, allowing a reliable abundance (and $T_{\rm eff}$) determination. IRS15SW will be further discussed in Sect. 6.3.

IRS15SW was studied by Najarro et al. (1997). We find a much larger $T_{\rm eff}$, essentially because we can rely on several He II lines and on the C IV/C III ratio (note the good fit of C lines in Fig. 13). We also find a much lower luminosity and a lower clumping corrected mass loss rate. The terminal velocity and H content are however similar (see Fig. 13 for a complete view of the He and H spectrum).

4.2.8. AFNWNW

AFNWNW is a WN7 star. Most of its lines are reasonably well reproduced by our best fit model (see Fig. 14). The main problems are the too weak He I 2.058 μm line and the too narrow He I/He II complex at 2.18–2.19 μm. Note however that the S/N ratio is rather low, preventing an accurate determination of the physical parameters. The absence of C IV emission indicates an upper limit of 10^{-4} for C/He. Note that our best fit model is unclumped. We cannot derive the clumping factor from the observed spectrum due to the poor S/N ratio.

4.2.9. IRS34NW

IRS34NW is a WN7 star. It has narrower and weaker lines than AFNWNW, reflecting its weaker wind. The C IV lines indicate a slightly sub-solar C abundance (see best fit in Fig. 15). Together with the N content derived from N III lines, this reveals

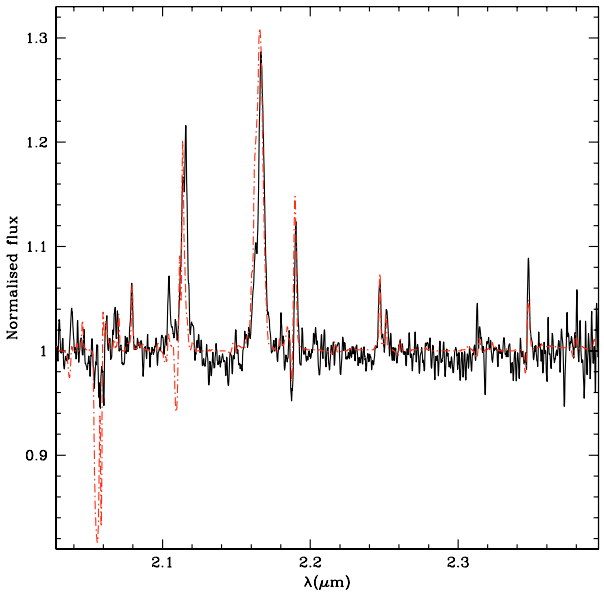

Fig. 15. Best fit (red dot-dashed line) to the observed K band spectrum of IRS34NW (WN7, black solid line).

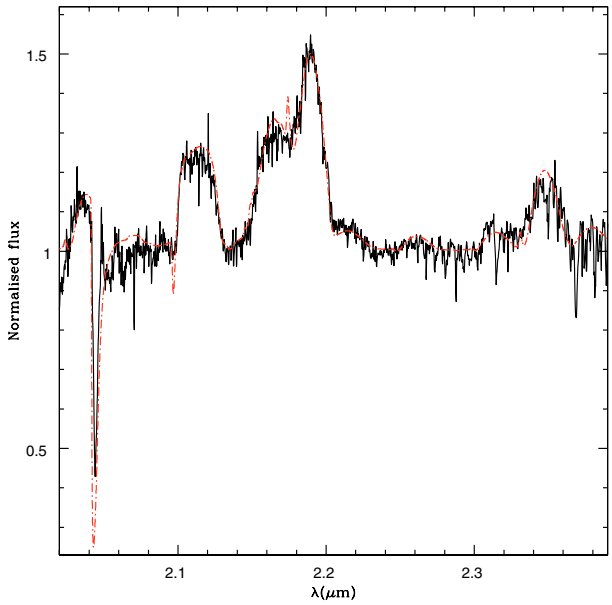

Fig. 16. Best fit (red dot-dashed line) of the observed K band spectrum of IRS16SE2 (WN5/6, black line).

an early stage of CNO processing (compared to AFNWNW which has no detectable C IV lines). IRS34NW still has a significant amount of Hydrogen. We conclude that IRS34NW is less evolved than AFNWNW in spite of a similar spectral type. This likely reflects different initial masses.

4.2.10. IRS16SE2

IRS16SE2 is the earliest WN star of our sample (WN5/6, see Paumard et al. 2006). Consequently, it also has the highest effective temperature (41 000 K) which is quite well constrained by the presence of both He I and He II lines in the K band spectrum. Helium is indeed doubly ionised in most of the atmosphere, except in the very outer part where it recombines, leading to the He I absorption trough near 2.044 μm. This feature being due to a blueshifted He I 2.058 μm absorption, we have a good estimate of the wind terminal velocity (2500 km s^{-1}). The absence of C IV emission around 2.08 μm – expected for such a large $T_{\rm eff}$ – sets an upper limit on the carbon abundance (C/He $\lesssim 10^{-4}$ by number), indicating CNO processing.

Crowther & Smith (1996) studied two WN6 stars with K band spectra very similar to IRS16SE2. Their results are in excellent agreement with the present ones: $T_\star \sim 55\,000$ K, $\log \frac{L}{L_\odot} \sim 5.4$ and $\log \frac{\dot{M}}{\sqrt{f}} \sim -3.9$. Since Crowther & Smith (1996) found no difference between their IR analysis and optical results, we are confident that the parameters we derive for IRS16SE2 for pure IR diagnostics are reliable.

4.3. WC9 stars

Here, the stellar and wind parameters of three WC9 stars are derived. One important word of caution is necessary though. WC9 stars are often associated with dust (Williams et al. 1987). The origin of this dust is not completely understood, but wind-wind interaction in binary systems is the favoured mechanism. Observation of dust spirals (also named "pinwheels") around several WC9 stars strongly support this scenario (Tuthill et al. 1999). Recent observations of the "Cocoon stars" after which the Quintuplet cluster was named showed such pinwheels (Tuthill et al. 2006).

The presence of dust in WC9 stars complicates the analysis of their IR spectra since it produces an additional emission which adds to the stellar+wind continuum. In practice, if WC9 stars are analysed under the assumption that they are dust-free, their continuum is over-estimated. Consequently, when normalizing their spectra, lines appear weaker. This implies under-estimates of the mass loss rates and abundances. In addition, the derived luminosity is over-estimated since the total continuum is composed of both the stellar+wind continuum and the dust emission. Note however that $T_{\rm eff}$ estimates are less affected, since the ratio of lines is only weakly affected by the presence of dust.

In the following, we discuss for each star the observational evidence for dust and the reliability of the derived parameters.

4.3.1. IRS7W

L-band observations of IRS7W were recently performed by Moultaka et al. (2005) [2]. Inspection of their Table 1 shows that the colors of IRS7W are consistent with the extinction law of the GC, at least in the HKL bands. A possible excess emission is only seen in the M band due to a red $L-M$ color. Consequently, we think that our modelling, restricted to the $H+K$ band spectrum, is not hampered by any dust emission. The derived parameters can be trusted within their error bars.

Our best fit is shown in Fig. 17. The effective temperature is relatively well constrained by the presence of several He II lines as well as C IV and C III features. The main discrepancy is once again the too weak He I 2.058 μm in our model. In addition, we note the two unidentified lines at 2.140 and 2.224 μm as in WN/C stars.

[2] IRS7W is their WR2 star, and not WR1 as they claim. Their WR1 star is IRS7SW.

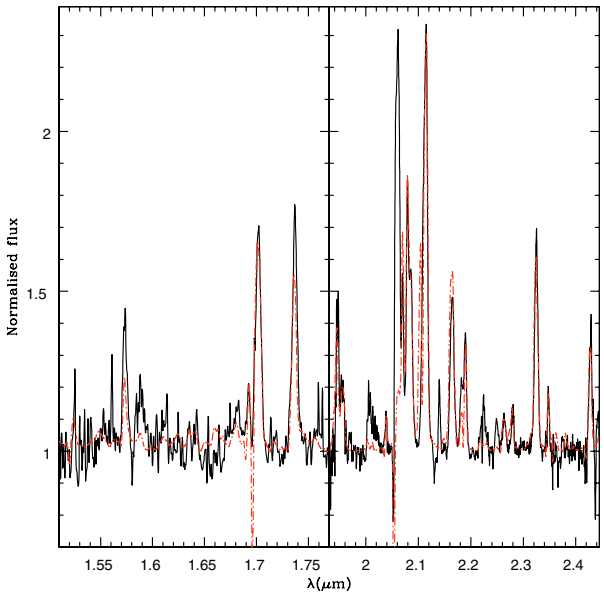

Fig. 17. Best fit (red dot-dashed line) of the observed H and K band spectra of IRS7W (WC9, black solid line).

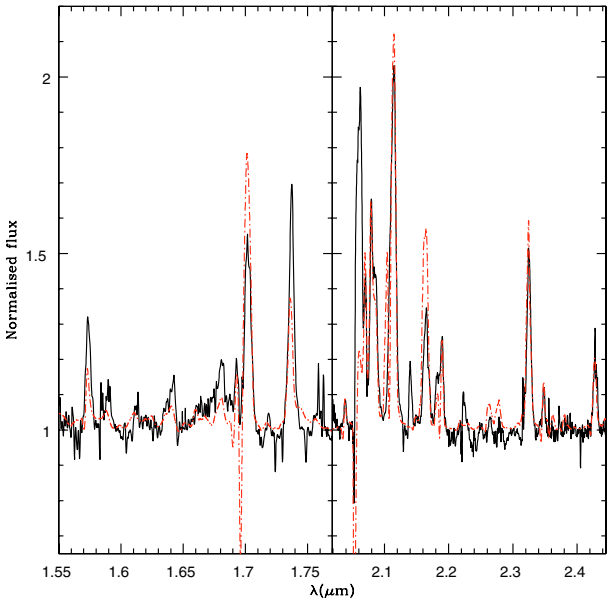

Fig. 18. Best fit (red dot-dashed line) of the observed $H + K$ band spectrum of IRS7SE (WC9, black solid line).

4.3.2. IRS7SE

IRS7SE is a WC9 star very similar to IRS7W. Unfortunately, we do not have any information on its photometry (except for the K-band). We are thus not able to check the possible contamination by dust. Adopting a conservative approach, we consider that our results are only limits (lower for $\dot{M}$ and the C abundance, upper for $\log \frac{L}{L_\odot}$). Figure 18 shows a fit of similar quality compared to IRS7W, with the same caveats (He I 2.058 μm, unidentified lines).

4.3.3. IRS13E4

Maillard et al. (2004) presented a detailed investigation of the stellar content of IRS13E. Using *HKL* photometry, they report the discovery of several very red sources in addition to the bright components IRS13E2 and IRS13E4. They interpret these sources as dusty Wolf-Rayet stars. Unfortunately, IRS3E4 is not detected in their L band images, so that the presence of a dust component in the spectrum of the WC9 star cannot be tested. It is however interesting to note that IRS13E2, the WN8 star analysed in Sect. 4.2.5, has a quite large $K - L$ color. The entire cluster IRS13E is also known to be at the top of a very prominent gas stream in L band (Clénet et al. 2004). Taken together, these arguments indicate that the stars of IRS13E may well all bathe in a continuum emission due to hot dust. We thus conclude that their derived parameters must be regarded as only indicative (see also Sect. 6.5).

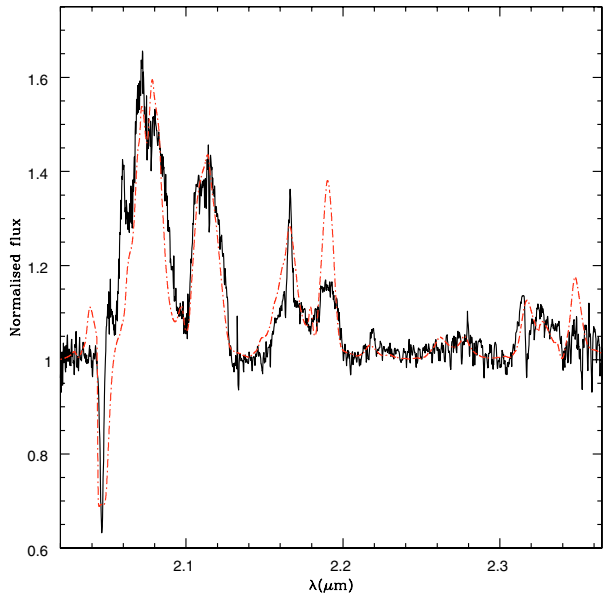

Fig. 19. Tentative fit (red dot-dashed line)of the K band spectra of the IRS13E4 (WC9, black solid line). See text for discussion of the discrepancies.

With this restriction in mind, we show a tentative fit of the spectrum of the WC9 star IRS13E4 in Fig. 19. The main C lines are reasonably well reproduced by our model. However, the He I 2.184 μm and He II 2.189 μm lines, while having the right line ratio, are too strong. Reducing them would require a reduction of the mass loss rate. This is at the cost of a reduction of the C lines (which could be compensated by an increase in the C abundance), *and* of a modification of the shape of the lines. With lower $\dot{M}$, lines get narrower and more centrally peaked because the density decreases. In conclusion, and given the above discussion, we argue that the near-IR spectrum of IRS13E4 is certainly contaminated by dust emission. Such a component could explain that the He I and He II lines are too weak (being diluted). Carbon lines are also certainly diluted, so that our C abundance estimate is likely a lower limit. We also probably over-estimate the total luminosity.

4.4. OB supergiants

Due to the rather limited signal to noise ratio of most of the spectra of the OB stars known in the central cluster (S/N of the order of a few tens on average), we have restricted ourselves to a general study of the properties of these stars. For that, we have used the average spectra of 10 supergiants presented in Paumard et al. (2006). Hence, we have derived average stellar and wind parameters for this population of OB stars.

Figure 20 shows the best fit model. The main parameters used for this model are: $T_{\rm eff}$ = 27 500 K, $\log g$ = 3.25, $\log \frac{L}{L_\odot}$ = 5.33, $\dot{M}$ = 3 × 10^{-7} $M_\odot$ yr^{-1}, v_∞ = 1850 km s^{-1}, X(He) = 0.3 and $v_{\rm turb}$ = 15 km s^{-1}. Additionally, a rotational velocity of ∼100 km s^{-1} could be estimated from the overall shape of all absorption lines[3]. The effective temperature is very difficult to constrain, just as in the Ofpe/WN9 stars studied previously. We can only put a constraint on the upper limit of $T_{\rm eff}$ from the absence of He II lines, especially He II 2.189 μm. This upper limit is of around 32 000 K. Giving a lower limit is more challenging. We tried several values between 25 000 and 32 500 K. This range is thought to be appropriate since all stars contributing to our average spectrum are late O / early B supergiants. For these types of stars, $T_{\rm eff}$ is expected to be around 25 000–30 000 K (Martins et al. 2005). Reasonable fits could be obtained for these different $T_{\rm eff}$. As we have no diagnostic to better constrain $T_{\rm eff}$, we finally adopted 27 500 K as a typical value. For the luminosity, we also adopted $\log \frac{L}{L_\odot}$ = 5.3 since this is typical of late O supergiants (e.g. Martins et al. 2005).

The mass loss rate is not strongly constrained either since most lines are seen in absorption and do not appear to be filled by wind emission. Here too, an upper limit on $\dot{M}$ of a few 10^{-6} $M_\odot$ yr^{-1} can be given, above which Br$_\gamma$ cannot be reproduced any more.

Finally, the He abundance is tentatively constrained from the strength of He I 2.112 μm, He I 2.150 μm, He I 2.161 μm and He I 2.184 μm. The strength of these lines not only depends on the He content, but also on the microturbulent velocity. The slope of the velocity law (the β parameter) plays a role too. As we have no independent way of determining all these parameters, we tried different combinations with reasonable values ($10 < v_{\rm turb} < 20$ km s^{-1}, $1.0 < \beta < 2.0$). In the end, we found that good fits could be achieved for He/H ratios in the range 0.2–0.35. This value will be discussed in Sect. 9. Finally, we stress that we do not reproduce the 2.115 μm emission. As discussed in Sect. 4.1.1, this line is not clearly identified and we did not try to fit it.

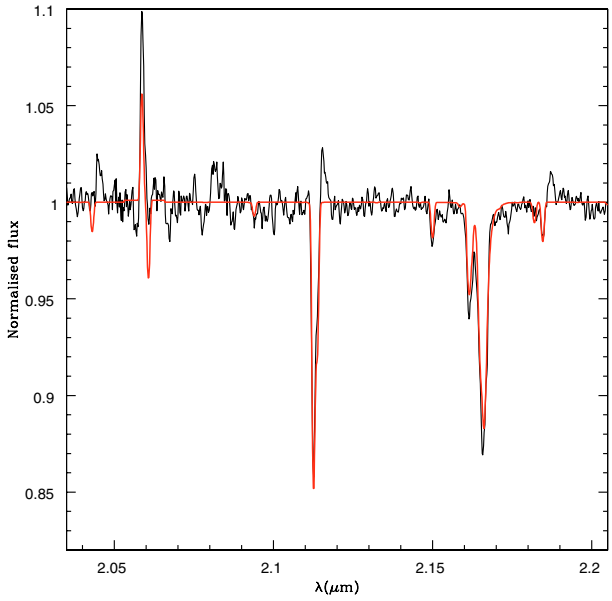

Fig. 20. Best fit (red solid line) of the average spectrum of the 10 supergiants (see Paumard et al. 2006).

5. Ionising radiation in the Galactic Center

One of the crucial issues revealed by early studies of the Galactic Center was the apparent incompatibility between the ionisation of the gas and the ionising flux provided by the population of massive stars. This was highlighted by Najarro et al. (1997) and more recently by Lutz (1999) in a detailed analysis of ISO observations (see also Thornley et al. 2000). In view of our new quantitative analysis, we argue that this issue is solved. Since this is an important result, we give a detailed explanation of the different aspects of the problem together with the proposed solutions.

5.1. H and HeI ionising photons

The first part of the "ionisation problem" concerns the total number of H and He I ionising photons produced by the GC massive stars (i.e. ionising photons short-ward of 912 Å – $Q_{\rm H}$ – and 504 Å – $Q_{\rm He\,I}$ –). Nebular emission from the central H II region was used to constrain the various ionising fluxes. Radio measurements of the free-free continuum by Ekers et al. (1983) showed that $Q_{\rm H}$ = $10^{50.4\pm0.3}$ s^{-1} (see also Genzel et al. 1994). Later, Krabbe et al. (1991) derived $Q_{\rm He\,I} \sim 10^{48.4}$ s^{-1} from a study of the nebular He I 2.058 μm emission. These measurements could then be compared to the results of the quantitative modeling of the stellar properties of the "He I" stars by Najarro et al. (1997). Their conclusion was that the "He I" stars provided enough H ionising photons, but failed by several orders of magnitude to produce the extreme UV flux required to account for the nebular He ionisation. An underlying population of stars hotter than the "He I" stars but not detected was suspected to be responsible for this harder flux.

Such a population has recently reported by Paumard et al. (2006). Hence, a re-estimate of the ionising power of the central cluster is required. Table 2 gives $Q_{\rm H}$ and $Q_{\rm He\,I}$ for the stars analysed in the present paper. In addition to these, Paumard et al. (2006) identified 15 other evolved massive stars and 59 OB stars. To estimate the total ionisation flux delivered by this population we used the following approach: for the WC9 stars not analysed here, we adopted the ionising fluxes of Smith et al. (2002) using their model WC number 3; for the 2 Ofpe/WN9 stars IRS16NE and IRS16SW, we adopted the parameters of IRS16C; for the WN7 stars not studied, we adopted the values of AFNWNW, another WN7 star included in our sample; finally, for the O stars, we adopted the calibration of Martins et al. (2005) (see their Table 4). Since all supergiants have a spectral type between O8.5 and B2 but some of them suffer from a classification uncertainty of up to 2 spectral sub-types, we adopted the ionising flux of a O9.5I star as typical of the GC supergiants. As for O dwarfs, the values of $Q_{\rm H}$ and $Q_{\rm He\,I}$ of Martins et al. (2005) for a O9.5V star were chosen. For the B dwarfs, we simply adopted a value ten times smaller than for OV stars. This is a rough approximation which however has very little impact on the final result, B stars providing a negligible ionising flux. This leaves us with the following numbers: $Q_{\rm H}$ = 6.0 × 10^{50} s^{-1} and $Q_{\rm He\,I}$ = 2.3 × 10^{49} s^{-1} (or $\log Q_{\rm H}$ = 50.8 and $\log Q_{\rm He\,I}$ = 49.4). The contribution of the different classes of stars are gathered in Table 3. We thus conclude that not only the H ionising flux but also the He I ionising flux required to reproduce the nebular emission can be provided by the population of massive stars. In fact, they may even produce slightly more ionising photons, indicating that the

[3] For that, the model spectra were convolved to take into account both the instrumental resolution and a rotational broadening represented by a simple Gaussian function.

Table 2. Derived stellar and wind parameters. The typical errors are: ±3000 K on temperatures (±6000 K for Ofpe/WN9 stars), ±0.2 dex on $\log \frac{L}{L_\odot}$ and $\log \dot{M}$, 100 km s^{-1} on terminal velocities and ±30% on abundances (except special cases; see comments on individual stars).

Star	ST	T_* [K]	$T_{\rm eff}$ [K]	$\log \frac{L}{L_\odot}$	R_* [$R_\odot$]	$R_{2/3}$ [$R_\odot$]	M_K	$\log \dot{M}$ [$M_\odot$ yr^{-1}]	f_∞	v_∞ [km s^{-1}]	H/He #	C/He #	X(N)	M [$M_\odot$]	$\log Q_{\rm H}$ [s^{-1}]	$\log Q_{\rm He\,I}$ [s^{-1}]
34W	Ofpe/WN9	23 000	19 500	5.5	35.9	49.3	–6.11	–4.88	1.0	650	4.0	–	–	–	48.32	47.64
16NW	Ofpe/WN9	20 000	17 500	5.9	59.1	75.8	–6.80	–4.95	1.0	600	5.0	–	–	–	48.04	47.35
16C	Ofpe/WN9	21 500	19 500	5.9	63.9	79.5	–7.05	–4.65	1.0	650	2.5	–	–	–	48.76	47.60
33E	Ofpe/WN9	20 000	18 000	5.75	63.9	75.9	–6.85	–4.80	1.0	450	4.0	–	–	–	48.26	47.60
AF	Ofpe/WN9	23 000	21 000	5.3	28.1	34.5	–5.77	–4.75	0.1	700	2.0	–	–	–	48.06	47.82
15NE	WN8	34 500	33 000	5.25	11.9	13.0	–4.65	–4.70	0.1	800	0.0	$<1 \times 10^{-4}$	0.0137	12.6	48.56	47.47
AFNW	WN8	37 000	33 000	5.5	13.9	17.5	–5.19	–4.50	0.1	800	0.1	$<1 \times 10^{-4}$	0.0326	18.6	49.14	47.60
9W	WN8	40 500	32 000	5.4	10.2	16.4	–5.20	–4.35	0.1	1100	0.1	$<5 \times 10^{-5}$	0.0133	15.8	49.11	47.79
7E2	WN8	37 500	34 500	5.2	9.5	11.1	–4.25	–4.80	0.1	900	0.0	$<8 \times 10^{-5}$	0.0137	11.7	48.88	47.70
13E2	WN8	29 000	29 000	6.1	44.7	45.0	–6.55	–4.35	0.1	750	0.1	$<3 \times 10^{-4}$	0.0167	82.5	49.49	47.61
7SW	WN8/WC9	34 500	33 000	5.55	16.8	18.0	–5.19	–4.70	0.1	900	0.0	0.005	0.0135	18.6	49.15	47.66
15SW	WN8/WC9	39 000	35 000	5.1	7.9	9.7	–4.36	–4.80	0.1	900	0.0	0.013	0.0229	10.3	48.77	47.83
AFNWNW	WN7	36 500	28 500	5.25	10.7	17.2	–4.59	–3.95	1.0	1800	0.1	$<1 \times 10^{-4}$	–	12.6	48.87	47.77
34NW	WN7	34 000	33 000	5.6	18.2	19.3	–4.71	–5.30	0.1	750	1.0	$1.5\ 10^{-4}$	0.0069	–	49.25	48.13
16SE2	WN5/6	53 000	41 000	5.45	6.4	10.5	–5.03	–4.15	0.1	2500	0.0	$<1 \times 10^{-4}$	–	17.2	49.24	48.51
7W	WC9	47 500	39 000	5.1	5.3	7.8	–3.79	–5.0	0.1	1000	0.0	0.06	–	10.3	48.86	47.80
7SE	WC9	44 500	36 500	5.15	6.4	9.5	–4.03	–4.90	0.1	1000	0.0	0.04	–	11.0	48.88	47.82
13E4	WC9	42 500	37 500	5.8	14.7	18.7	–5.44	–4.30	1.0	2200	0.0	0.02	–	45.0	49.56	48.47

H II region might be density bounded. A final comment on the total He I ionising flux is needed. Krabbe et al. (1991) state that $\log Q_{\rm He\,I} = 48.4$ s^{-1}, but also that $Q_{\rm He\,I}/Q_{\rm H} = 0.06$. We find $Q_{\rm He\,I}/Q_{\rm H} = 0.04$, in very good agreement. The difference in the absolute $Q_{\rm He\,I}$ values between our study and Krabbe et al. (1991) is their lower reference $Q_{\rm H}$ ($\log Q_{\rm H} = 49.6$).

At this point, a comment on the contribution of the "He I" stars is necessary. Najarro et al. (1997) showed that the 8 stars they analysed could account for most of the ionising radiation of the region. We see that with the current estimate, this conclusion would not be valid. Why is that? The answer is rooted in 1) our lower bolometric luminosities and 2) the inclusion of line-blanketing in the atmosphere models. This ingredient was not available at the time of the Najarro et al. (1997) study. Test models reveal that in such stars, line-blanketing effects lead to a large redistribution of the blocked UV flux to longer wavelengths, mainly above 912 Å. Consequently, $Q_{\rm H}$ is reduced significantly.

5.2. Ionising radiation and stellar population

The second important issue concerning the ionising radiation in the Galactic Center was highlighted by Lutz (1999). In his study of nebular fine structure mid-IR lines of metals observed with ISO, Lutz pointed out that stellar evolution appears to fail to explain the GC massive stellar population. This claim was based on computations of population synthesis models for a single burst of star formation and a standard Salpeter IMF. After 7 Myr, the age of the population thought to be appropriate at that time, the fraction of the total ionising luminosity provided by the part of the HR diagram where the "He I" stars are lying ($\log T_{\rm star} < 4.5$ and Ł > 5.75) was of the order of 1%. This was at odds with the results of Najarro et al. (1997) who argued that these stars could account for more than half the total ionising luminosity. This discrepancy lead Lutz (1999) to the conclusion that stellar evolution – indirectly tested here through synthesis population models – was not producing enough cool stars or equivalently that the time spent by a massive star in the cool part of its track was much too short.

This statement is no longer valid. Only six stars analysed here have $\log T_{\rm star} < 4.5$ and $\log \frac{L}{L_\odot} > 5.75$. And this is in the case we include IRS13E2 for which we only have an upper limit on $\log \frac{L}{L_\odot}$. To these four stars, we need to add the binary IRS16SW and the binary candidate IRS16NE. Both stars likely have properties similar to IRS16C. In total, the H ionising flux of these stars represents about 9% of the total $Q_{\rm H}$. This is an upper limit due to the possible overestimate of IRS13E2's luminosity. If we exclude IRS13E2, the remaining 7 stars contribute only 4% of $Q_{\rm H}^{\rm total}$. This is in excellent agreement with what is expected from a burst of star formation after 7 Myr (which is within the age range now stated for the population, see Paumard et al. 2006). Once again, this is mainly due to the recent discovery of a hot population of OB and Wolf-Rayet stars responsible for the majority of the ionising luminosity. Table 3 shows that the OB supergiants and Wolf-Rayet stars contribute more than 90% of the ionising flux. The main conclusion is that standard stellar evolution – used in population synthesis models – is able to account for the GC massive stars.

5.3. Mid-IR nebular Ne lines

The third problem with the ionisation of the Galactic Center region was also pointed out by Lutz (1999) (see also Thornley et al. 2000). It concerned the low ionisation of the local gas as derived from the ratio of fine structure mid-IR lines of different ionisation states of Ne, namely Ne III 15.5 μm and Ne II 12.8 μm. ISO observations revealed that [Ne III]/[Ne II] was 0.05. Using the SED predicted by the synthesis population model described in the previous section as an input of a photoionisation model performed with the code CLOUDY (Ferland et al. 1998), Lutz revealed that after 7 Myr, [Ne III]/[Ne II] was still as large as 1 to 2, or a factor 50 to 100 more than the observed value.

To investigate this issue, we have performed photoionisation models with CLOUDY (version C06.02). As an input SED, we have simply added all individual SEDs computed for the stars presently studied. For those stars which were not explicitly treated here, we have adopted the SEDs of Martins et al. (2005) or those of similar stars present in the current sample. Adopting

Table 3. Contribution of the different types of stars to the ionising fluxes.

Type of star	Number of stars	$Q_{\rm H}$ [s^{-1}]	% $Q_{\rm H}$ total	$Q_{\rm He\,I}$ [s^{-1}]	% $Q_{\rm He\,I}$ total
OB V	23	3.1×10^{48}	0.5	2.6×10^{46}	0.1
OB I	30	3.0×10^{50}	50.0	6.7×10^{48}	29.1
Ofpe/WN9	8	2.5×10^{49}	4.2	3.4×10^{48}	14.8
WN	9	1.1×10^{50}	18.3	7.0×10^{48}	30.4
WN/C	2	2.0×10^{49}	3.3	1.1×10^{48}	4.8
WC	13	1.5×10^{50}	25.0	4.7×10^{48}	20.4
Total		6.0×10^{50}		2.3×10^{49}	

the same density as Lutz (1999) (3000 cm^{-3}) and our total ionising flux implies an ionisation parameter $\log U = -0.6$[4]. With these values, we obtain a ratio [Ne III]/[Ne II] of 0.9–1.7 depending on the geometry. This is still larger than the observed value (0.05). Note however that if we use the ionisation parameter as Lutz (1999) ($\log U = -1$), we get [Ne III]/[Ne II] ∼ 0.5–0.7. This is a factor 2–3 lower than the values of Lutz.

How can we explain the still large values of [Ne III]/[Ne II]? One possibility is that we underestimate the density. There is evidence that values as large as 10^{4-5} cm^{-3} are required to produce [O I], [O III] and [Fe II] lines (Genzel et al. 1984, 1985). Using such large values (and the corresponding ionisation parameter, $\log U = -1.2$ and -1.6), CLOUDY models with our total stellar SED give [Ne III]/[Ne II] ∼ 0.5 (for 10^4 cm^{-3}) and ∼0.1 (for 10^5 cm^{-3}). This is in better agreement with the observed ratio, although still a factor 2–10 too large. Shields & Ferland (1994) argued that the nebular spectrum of the Galactic Center could be reproduced only if several gas components with different densities were involved. In view of the present result, it may well be that the Ne ionisation requires a large density material (we can reproduce the observed [Ne III]/[Ne II] ratio for a density of 3×10^5 cm^{-3}).

Another explanation of the large theoretical [Ne III]/[Ne II] ratio could be that we still overestimate the flux at 41 eV, i.e. the Ne II ionisation energy probed by the [Ne III]/[Ne II] ratio. This part of the spectrum is quite sensitive to blanketing effects. A slight increase in metallicity could lead to a reduced flux and consequently a lower [Ne III]/[Ne II] ratio (e.g. Morisset et al. 2004).

One may also wonder what type of star contributes significant flux at 41 eV. It turns out that the total SED is completely dominated by a single star at this energy: the hot WN5/6 star IRS16SE2. To test the influence of this star on the ionisation of the GC gas, we removed its contribution to the total SED and ran test CLOUDY models. Amazingly, for a density of 3000 cm^{-3} (and $\log U = -0.6$), the [Ne III]/[Ne II] ratio drops to 0.008, less than the observed value. This shows that this ratio is extremely sensitive to the local radiation field. One can imagine that most of the ionised gas is not illuminated by the IRS16SE2 radiation due to shielding by local structures in molecular clouds. In that case, the remaining radiation field is soft enough to maintain a low [Ne III]/[Ne II] ratio.

In conclusion, one could say that a revised nebular modelling taking into account both the spatial distribution of the gas and of the ionising sources is required to solve the Ne ionisation problem. This is well beyond the scope of the present paper.

[4] the ionisation parameter is defined by $U = \frac{Q_{\rm H}}{4\pi r^2 nc}$ where r is the distance to the ionising source (chosen to be 0.5 pc in our case) and n is the density.

6. Stellar evolution in the Galactic Center

In this section we discuss, in view of the results of our quantitative analysis, the evolution of massive stars beyond the main sequence. It is generally accepted that stars in the mass range 25–60 $M_\odot$ evolve from O stars to WN H-poor stars through a LBV and/or red supergiant phase before becoming WC stars (for $M > 40$ $M_\odot$). In the following, we refine this scenario in the particular case of the GC, establishing a plausible evolutionary sequence between Ofpe/WN9, WN8 and WN/C stars (Sects. 6.1, 6.2, 6.3). We also quantitatively compare the position of the GC Wolf-Rayet stars in the HR diagram to evolutionary tracks including rotation (Sect. 6.4). Finally we discuss the properties of the IRS13E cluster stars (6.5).

6.1. Ofpe/WN9 stars

In the present study, we have analysed five stars classified Ofpe/WN9 by Paumard et al. (2006). Among these five stars, three have been studied by Najarro et al. (1997): IRS16C, IRS16NW and AF. Compared to the Najarro et al. analysis, we find a similar range of luminosities (although for IRS16C our luminosity is lower) and the same terminal velocities (within the uncertainty). The effective temperatures are higher in our study, partly due to the inclusion of line-blanketing in our models as already discussed. Nevertheless, $T_{\rm eff}$ remains poorly constrained so that the range of acceptable values overlap with the temperatures of Najarro et al. (1997). As a consequence of the hotter $T_{\rm eff}$, our radii are smaller. But the main differences concern 1) the mass loss rates and 2) the He content. Both parameters are linked to some extent: when fitting He I 2.058 μm, He I 2.112 μm and Br_γ, adopting a larger He/H content will require a larger $\dot{M}$ in order to reproduce the level of Br_γ emission. Of course, in that case He I 2.058 μm and He I 2.112 μm get stronger too. But their absolute strength is also controlled by the He ionisation which in turn depends on the effective temperature and the line-blanketing effect. Since we used more realistic atmosphere models as well as better spectra (higher S/N ratio and spectral resolution, good correction from nebular emission), we argue that our derived parameters represent an improvement over the result of Najarro et al. (1997). In practice, we find values of $\dot{M}$ 3 to 10 times lower than Najarro et al., and much lower He contents (He/H ∼ 0.2–0.5 compared to 1.3–3.0).

These revised parameters are important for assessing the evolutionary status of the Ofpe/WN9 stars (see next section). They are also very interesting since they bring the GC Ofpe/WN9 stars closer to other Galactic and LMC stars of this type. Crowther & Smith (1997) analysed a sample of LMC Ofpe/WN9 stars and found that their He content was much smaller than in the GC stars, which was tentatively attributed to possible metallicity effects. Our new values are in better

agreement with the Crowther et al. measurement, showing that the LMC and GC Ofpe/WN9 stars are chemically similar. In contrast, Pasquali et al. (1997) found He/H ∼ 0.5 (by number) for a sample of LMC Ofpe/WN9 stars partly overlapping with the Crowther et al. sample. These He contents are only marginally larger than ours, and are certainly lower than the values of Najarro et al. (1997). Concerning the mass loss rates, we find that on average $\dot{M}$ is systematically smaller than in the Crowther & Smith (1997) and Pasquali et al. (1997) studies. This difference is surprising since the lower metallicity of the LMC should lead to *lower* mass loss rates. Combined with the slightly larger He content, this may be an indication of a more advanced evolution. Another indicator points to the same conclusion: the terminal velocities of the GC Ofpe/WN9 stars are usually larger than for stars of the same spectral type (see Pasquali et al. 1997; Bresolin et al. 2002). Interestingly enough, the only Galactic star of this type studied by Crowther & Smith (1997) had a much larger v_∞ than the LMC stars. Schaerer (1996) explained such a trend by a more advanced evolution in the Ofpe/WN9 phase for stars in the LMC, with the consequence of greater proximity to the Eddington limit and implying a lower terminal velocity.

In conclusion, in view of our study, the class of Ofpe/WN9 seems to be more homogeneous than previously believed. The difference between GC and LMC Ofpe/WN9 stars is likely due to a different state of chemical evolution: massive stars become Ofpe/WN9 stars later in a low Z environment such as the LMC, mainly due to lower mass loss rates.

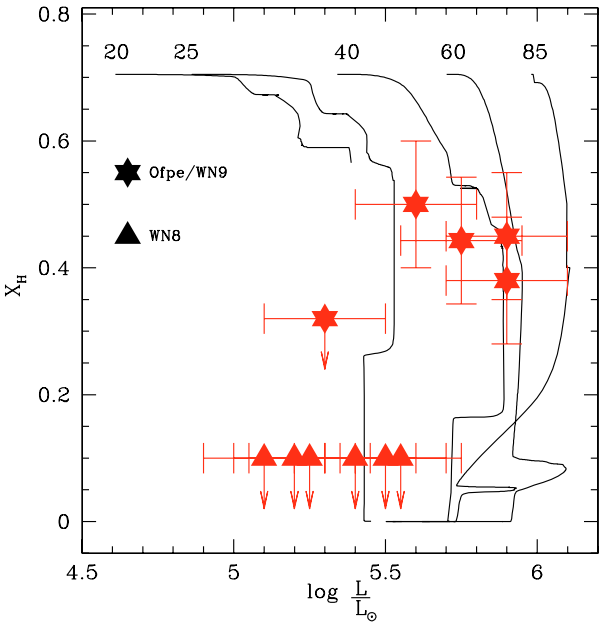

Fig. 21. Hydrogen mass fraction as a function of luminosity. Solid lines are the Geneva evolutionary tracks with rotation and $Z = Z_\odot$ (Meynet & Maeder 2005). The ZAMS masses for each track are indicated. Stars show the position of the Ofpe/WN9 stars (IRS16C, IRS16NW, IRS33SE, IRS34W, AF) analysed here, while the triangles are the WN8 stars of our sample. The AF star lies at $\log \frac{L}{L_\odot} = 5.3$ and $X(\mathrm{H}) = 0.3$. See Sect. 6.4 for discussion.

6.2. An evolutionary link between Ofpe/WN9 and WN8 stars

On the basis of their K band morphology, all of the initial "He I" stars have been classified as either Ofpe/WN9 or WN8 stars by Paumard et al. (2006). These two spectral types are indeed characteristic of relatively cool evolved massive stars. In the K band, they are defined by strong He I and Br$_\gamma$ emission lines. The relative intensity of these different lines is similar in both spectral types: He I 2.058 μm is usually stronger than Br$_\gamma$, while He I 2.112 μm is weaker or of equal strength. The main differences are 1) the shape of the lines (Ofpe/WN9 stars show P-Cygni profiles in the He I lines, while WN8 stars have strong pure emission lines); 2) their width (WN8 stars have broader lines); 3) their absolute strength (stronger lines in WN8 stars); and 4) the presence of weak HeII lines in WN8 stars. Inspection of Table 2 reveals that quantitatively, these morphological differences are due to larger mass loss rates (and to a lesser extent wind terminal velocities) as well as higher effective temperatures for WN8 stars. Indeed, $T_{\rm eff}$ ranges from 30 000 to 41 000 K for WN8 stars, while they are lower than 30 000 K for Ofpe/WN9 stars. Mass loss rates are ∼2–4 times smaller in Ofpe/WN9 stars. Luminosities are also slightly lower in WN8 stars. This comparison indicates that Ofpe/WN9 stars and WN8 stars may be physically related and may well represent consecutive phases of a single evolutionary sequence.

Figure 21 displays the H content as a function of luminosity in evolutionary models (solid lines) and shows the position of the Ofpe/WN9 and WN8 stars. It is clear that both types of stars gather in different parts of the diagram: Ofpe/WN9 stars still show a significant amount of hydrogen in their atmospheres whereas WN8 stars are mainly H free. This can be interpreted as an evolutionary sequence where Ofpe/WN9 stars evolve into WN8 stars. Such a scenario would be consistent with the properties reported above. Ofpe/WN9 stars could well be on the cool part of an evolutionary track. This track will then loop back to the hot part of the HR diagram. As a star follows this track, it evolves chemically, gets hotter and strengthens its wind on its way to the WR phase. The hotter $T_{\rm eff}$ and larger $\dot{M}$ explains the appearance of HeII lines and the stronger emission lines, and the lower H content reveals the chemical evolution of the star. In this scenario, the AF star could be in an intermediate state. Its spectral morphology is similar to WN8 stars except that it does not show HeII lines, indicating a relatively cool $T_{\rm eff}$ (confirmed by the quantitative analysis, see Table 2). Its mass loss rate is also more typical of WN8 stars. In Fig. 21, the AF star lies in between the groups of Ofpe/WN9 and WN8 stars, with a H mass fraction $\lesssim$0.3. Hence, it is also more evolved than Ofpe/WN9 stars, but less than WN8 stars, and nicely fits in the evolutionary scenario we suggest.

Another argument in favour of this scenario is the variability of both types of objects. On the one hand, the Ofpe/WN9 stars in the Galactic Center have been claimed to be LBV candidates, or even LBVs in a quiescent phase (Paumard et al. 2004; Trippe et al. 2006). This is based on spectral similarities between these stars and objects elsewhere in the Galaxy and LMC known to be related to LBV stars. Besides, one of them – IRS34W – was shown to be photometrically variable on timescales of months-years. Trippe et al. (2006) interpreted that as a sign of obscuration by dust produced in material ejected in an LBV-type outburst of the star. On the other hand, WN8 stars are known to be the class of Wolf-Rayet stars experiencing the strongest variability (Antokhin et al. 1995; Marchenko et al. 1998). This high degree of variability may be related to the LBV phenomenon. A link between WN8 stars and LBVs is also favoured by the presence of LBV-like nebulosities around most of them (Crowther et al. 1995b).

We thus argue that the GC Ofpe/WN9 stars are precursors of WN8 stars, and are in a state closely related to the LBV phase. This picture is fully consistent with the scenario of

Crowther et al. (1995b), further extended by Crowther & Smith (1997): a 25–60 $M_\odot$ star evolves into a WN9-11 star (similar to Ofpe/WN9, see Crowther et al. 1995a) before experiencing a LBV phase and becoming a WN8 Wolf-Rayet star. The properties of the WN8 stars analysed by Crowther et al. (1995b) and Herald et al. (2001) are very similar to those of our sample WN8 stars. The only difference is a larger spread in H content: while we find all WN8 to be almost H free, Crowther et al. (1995b) have both H free stars and stars still showing a significant amount of hydrogen. Herald et al. (2001) also found $X(\mathrm{H}) \sim 20\%$ by mass. However, this H content remains much lower than in the GC Ofpe/WN9 stars. Hence, the suggested evolutionary scenario remains valid.

6.3. WN/C stars

WN/C stars are Wolf-Rayet stars showing both strong C and N lines (Massey & Grove 1989; Willis & Stickland 1990). Carbon is produced by the triple α reaction, while Nitrogen results mainly from CNO processing. It is widely accepted that WN/C stars are core He burning stars with a CNO-enriched envelope in which mixing processes have created a layer with both H and He burning products. When mass loss reveals this layer, the star turns into a WN/C star (Langer 1991; Meynet & Maeder 2003, 2005). Quantitatively, such WN/C stars have C/N ratios of the order 1.

For a long time, the fraction of WR stars in the WN/C state observed in the Galaxy has been difficult to explain with evolutionary models. Abundance profiles in such models were usually very steep in the transition region between H and He burning products, so that the region where both type of products were present was extremely thin. Consequently, it was quickly removed by the stellar wind, resulting in a very short lifetime of the WN/C phase. Consequently, the number of WN/C stars predicted by such models was much lower than the observed value. Significant improvements have been made in the last years mainly due to the inclusion of mixing processes triggered by rotation. Meynet & Maeder (2003) have shown that rotation created shallower abundance gradients in stellar interiors, increasing the size of the mixed H and He burning products. As a consequence, the lifetime of the WN/C phase is lengthened, resulting in a total number of WN/C stars in better agreement with observations.

What about the GC Wolf-Rayet population? Our analysis of IRS15SW and IRS7SW has revealed that they were significantly enriched in Carbon compared to other WN stars, leading to a classification as WN8/WC9 stars. Figure 22 shows the position of our sample stars in a $\log \mathrm{C/N} - \log \mathrm{C/He}$ diagram. It turns out that IRS15SW and IRS7SW lie in between WN stars (stars with low C content) and the C-rich WC9 stars. Their position is also in excellent agreement with WR8 and WR145, two WN/C stars studied by Crowther et al. (1995d), and with the prediction of evolutionary models. Hence we have a quantitative confirmation that IRS15SW and IRS7SW are core He burning objects on their way to a WC phase. Meynet & Maeder (2003) argue that only stars with initial masses in the range 30–60 $M_\odot$ go through the WN/C phase: more massive stars have very strong winds that quickly remove the CNO enriched envelope; lower mass stars have a too H-rich envelope and He burning products are too diluted. Estimates of the present-day masses of IRS15SW and IRS7SW from the mass luminosity relation of Heger & Langer (1996) for H free WR stars gives 10.3 and 20.0 $M_\odot$ respectively, implying that these stars have lost 30 to 80% of their mass through stellar winds.

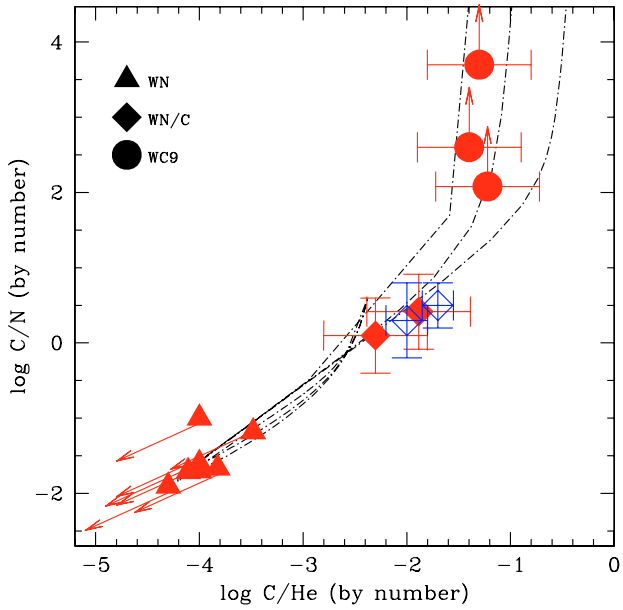

Fig. 22. $\log \mathrm{C/N}$ as a function of $\log \mathrm{C/He}$ (by number) from evolutionary tracks with rotation (dot-dashed line) from Meynet & Maeder (2005). Filled symbols are the WR stars analysed in the present paper (triangles: WN stars; diamonds: WN/C stars; circles: WC9 stars). Open diamonds are the WN/C stars WR8 and WR145 from Crowther et al. (1995d). IRS7SW and IRS15SW, the two WN/C stars of our sample, have C/N and C/He ratios very similar to WR8 and WR145. The GC WN stars all lie at $\log \mathrm{C/He} \lesssim -3$. For these stars, we have only upper limits on the C abundance, and consequently on $\log \mathrm{C/N}$ and $\log \mathrm{C/He}$. The WC9 stars analysed here have large C/He ratios and only lower limits on C/N since no N lines are present in the spectra and only an upper limit on the N abundances can be estimated.

If we compare the properties of IRS15SW and IRS7SW to WR8 and WR145 (see Crowther et al. 1995d), the luminosities are all similar, in the range $10^{5.1-5.5}$ $L_\odot$, which in turn implies that the present-day mass of these four objects are also very close (10–20 $M_\odot$). The clumping corrected mass loss rates are also similar, with $\log \dot{M}/\sqrt{f} \sim -4.3$. However, the terminal velocities of the GC stars are smaller than for WR8 and WR145 (700–800 $\mathrm{km\,s^{-1}}$ as opposed to 1390–1590 $\mathrm{km\,s^{-1}}$) as well as the stellar temperatures (32–37 kK vs. 41–48 kK). These differences reflect the different spectral types of the two samples: while the GC WN/C stars are late type WR stars (WN8/WC9), WR8 and WR145 are earlier (WN6/WC4, see Crowther et al. 1995d). Earlier WN and WC type stars have higher effective temperatures and larger terminal velocities (see Fig. 25). This can explain the observed trend: both types of stars (early and late WN/C stars) have the same luminosity but early WN/C stars are hotter, which implies that their radius is smaller. Consequently, their escape velocity, scaling as $(M/R)^{0.5}$, is larger (the present mass being approximately the same). Since the terminal velocity is directly proportional to the escape velocity, one naturally finds larger v_∞ in early WN/C stars.

We argue that the GC WN/C stars are most likely the descendents of WN8 stars. Their spectral morphology is extremely similar, except for the presence of C IV and C III lines in the WN/C stars. The quantitative analysis confirms their "twin" character: the ranges of values for $T_{\rm eff}$ luminosities, mass loss rates, terminal velocities, He and N content are the same for both WN8 and WN/C stars (see Table 2). The only possible exceptions are IRS13E2 (but see discussion in Sect. 6.5) and IRS9W. Figure 22 shows that the WN/C stars are more

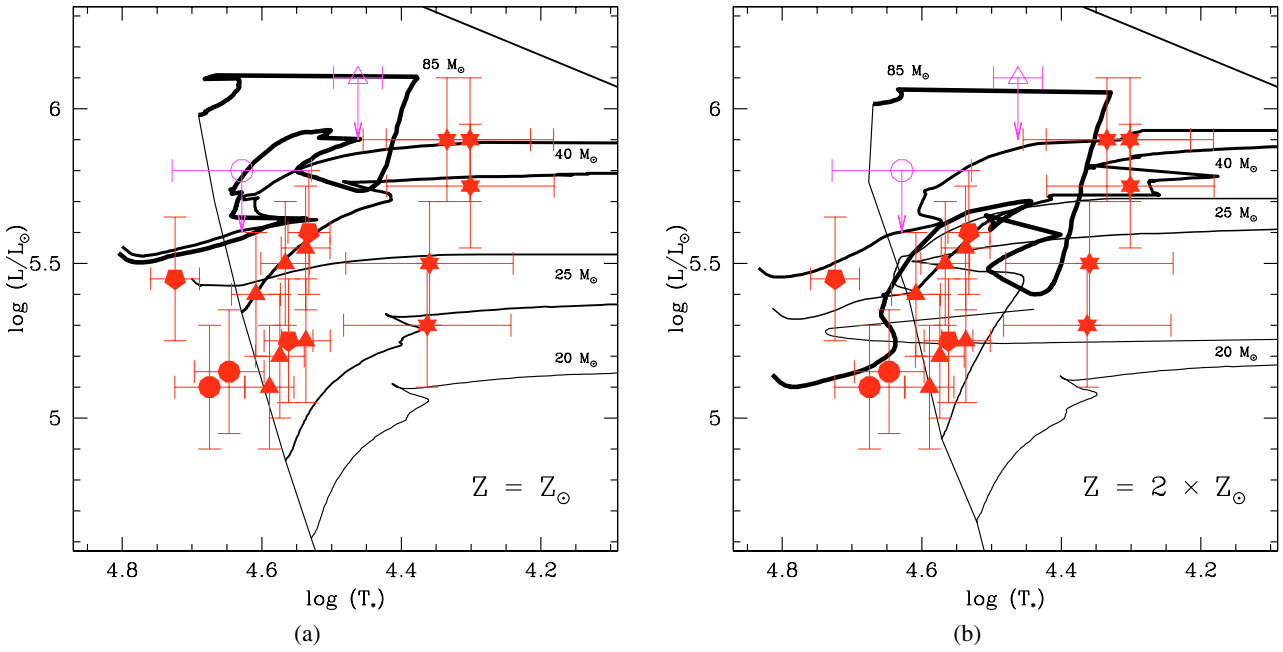

Fig. 23. HR diagram of WR stars in the GC. *Left*: solar metallicity tracks with rotation ($V \sin i$ = 300 km s^{-1} on the main sequence). *Right*: twice solar metallicity tracks including rotation. Star symbols are Ofpe/WN9 stars, triangles WN8 stars, pentagons WN5-7 stars and circles WC9 stars. Different line thickness indicates different evolutionary tracks (the thicker the line, the higher the mass). ZAMS masses are marked for each track. The Humphreys-Davidson limit is also shown in the right upper part of each diagram.

chemically evolved than WN stars. Hence, we conclude that most of the GC WN8 stars will go through a WN/C phase as two of them are currently doing.

Summarizing the last three sections, we argue that in the Galactic Center, stars with initial masses in the range 30–60 $M_\odot$ follow the evolutionary sequence

(Ofpe/WN9 $\rightleftharpoons$ LBV) $\rightarrow$ WN8 $\rightarrow$ WN/C

on their way to the supernova explosion. On the main sequence, they probably appear as mid/early O stars. After the WN/C phase, they most likely become late WC stars. Indeed the effective temperatures of WN/C stars are slightly lower than the WC9 stars of our sample. Hence, we can expect them to enter the WC sequence from the low ionisation (or equivalently the low $T_{\rm eff}$) side and appear as WC9 stars. The (Ofpe/WN9 $\rightleftharpoons$ LBV) sequence in the suggested scenario indicates that Ofpe/WN9 and LBV stars are closely inter-related and most likely represent different states of a single evolutionary phase (see discussion in Trippe et al. 2006).

6.4. Are stellar evolutionary tracks too luminous?

The direct comparison between derived parameters and evolutionary tracks by means of a classical HR diagram ($\log L - \log T_{\rm eff}$) is not straightforward for Wolf-Rayet stars. In evolutionary models, the "effective" temperature (noted $T_{\rm evol}$ in the present discussion) is defined at the outer boundary by Eq. (3). However, there is no atmosphere in such models and strictly speaking, the radius in this case (noted $R_{\rm evol}$) is not the one for which the optical depth is equal to 2/3 (exact definition of $T_{\rm eff}$). It corresponds more to a hydrostatic radius. In Wolf-Rayet stars, such a radius – for which the atmosphere is quasi-static – is at an optical depth much larger than 2/3. Said differently, $R_{2/3}$ for which $T_{\rm eff}$ can be defined is much larger than $R_{\rm evol}$. Consequently, $T_{\rm eff}$ is lower than $T_{\rm evol}$. To overcome this problem, one usually defines a radius $R_\star$ (and the corresponding temperature $T_\star$, see Eq. (3)) at an optical depth equal to 20. Such a radius is more comparable to $R_{\rm evol}$ so that $T_\star$ and $T_{\rm evol}$ can be directly compared.

In Fig. 23, we show the HR diagram built using $T_\star$ for our program stars (see Table 2). They are shown by the filled symbols (see next section for a discussion of the two stars represented by open symbols). The evolutionary tracks including rotation of Meynet & Maeder (2005) for solar metallicity (left) and twice solar metallicity (right) are overplotted. In the diagram at $Z = Z_\odot$, we clearly see that the Ofpe/WN9 stars populate the coolest region, while the more evolved Wolf-Rayet stars are hotter and, on average, less luminous. Qualitatively, this trend is similar to the 40 $M_\odot$ track: coming back from its redward extension, this track goes to lower temperatures. However, this track, as well as the ones for other masses, always remains at $\log L/L_\odot > 5.4$, in contrast to most of the Wolf-Rayet stars of our sample which have $5.1 < \log L/L_\odot < 5.5$. Hence, we see that quantitatively the solar metallicity evolutionary tracks do not seem to explain the evolution of the GC Wolf-Rayet stars. Note that this is independent of any definition of the temperature, since the problem is due to luminosities.

If we now focus on the HR diagram where the $Z = 2 \times Z_\odot$ metallicity tracks are plotted, we see that lower luminosities are reached. This is due to the stronger mass loss rates in these tracks which "peel off" the star more quickly, reducing its radius and consequently its luminosity. Does that mean that the GC stars have a supersolar metallicity? We will see in Sect. 7 that the question is still largely debated. The position of the GC Wolf-Rayet stars in the HR diagram may be an indication of a super-solar environment. But this can also be due to inadequate mass loss rates in evolutionary calculation at solar metallicity. If the amount of mass lost during the Wolf-Rayet phase is underestimated in such calculations, the tracks will be too luminous. Large $\dot{M}$ can be produced by a fast rotation (see Maeder & Meynet 2000), but the analysis of OB stars average spectrum

do not point to any particularly high $V \sin i$ (see Sect. 9). As long as the GC metallicity remains poorly constrained, a quantitative test of evolutionary tracks and their input parameters, such as mass loss rates, is thus not feasible. We will see in Sect. 7 that more work is needed to narrow the range of acceptable values for Z in the Galactic Center.

6.5. The stars of IRS13E

In the previous section, we have deliberately excluded two stars from the discussion: the ones represented by open symbols in Fig. 23. These stars are the two Wolf-Rayet components of the cluster IRS13E, namely IRS13E2 and IRS13E4. The reason is that they show peculiar properties compared to the bulk of the GC Wolf-Rayet stars. Take first IRS13E2. It is a WN8 star (see its spectrum in Fig. 11) with parameters in marginal agreement with the other WN8 stars of our sample, with the notable exception of its luminosity ($\log L/L_\odot = 6.1$) which is much larger than the range of values for WN8 stars (5.1–5.5, see Table 2 and Crowther et al. 1995b). The same statement is true for IRS13E4. It is a WC9 star but exceptionally bright: while most stars of this type have $\log L/L_\odot = 5.0$ (see an example in Crowther et al. 2006), IRS13E4 is nearly 10 times more luminous. In addition, it shows a large, although not unprecedented, terminal velocity (see Fig. 25).

How can we interpret these results? First, the most obvious explanation is binarity. IRS13E was initially thought to be a single star (Krabbe et al. 1991) before being resolved into several components (Maillard et al. 2004). The cluster is extremely compact and it is quite possible that the bright components might actually be multiple stars. But even with better spatially reduced images, it may not be sufficient to distinguish between the components of a massive binary. Spectrophotometric monitoring should then be used to test the binary hypothesis. So far, IRS13E2 and IRS13E4 (Figs. 11 and 19) do not show any sign of double line spectrum. In addition, photometric observations over the recent years (but with a very coarse sampling) show a flat light-curve for both stars (Trippe et al., in prep.). Better monitoring is required, but so far no clear evidence for binarity exists for IRS13E2 and IRS13En.

But the most important factor was mentioned in Sect. 4.3: dust contamination. There is evidence of a large dust content in IRS13E which may affect the infrared spectra of its stellar components. As a consequence, the luminosities are most likely upper limits. However, the luminosity difference between IRS13E4 and IRS7W is 0.7 dex, or a factor of 5. Assuming that both stars have the same luminosity and same spectral energy distribution, this means that the total K band flux is 5 times larger than the stellar+wind flux. This is exactly what is found by Crowther et al. (2006) in their analysis of the WC9 star HD164270: dust contributes 80% of the continuum. Note that their estimate is at 3 μm and not in the K-band, where dust contamination is smaller. But Crowther et al. (2006) also claim that HD164270 has a weak dust shell compared to other dusty WC stars. Hence, for a typical WC star a 80% dust contribution to the K band continuum is not unrealistic.

Although further high spatial resolution photometric data in the near/mid IR range are needed to establish the true SED of each component, it is likely that dust explains most of the peculiar properties of the IRS13E Wolf-Rayet stars.

7. Metallicity in the central parsec

We first present a determination of the global metallicity in the GC by means of WN stars, and we then discuss its effect on He I 2.058 μm.

7.1. Metallicity from N content of WN stars

Najarro et al. (2004) presented a new method for deriving metallicity in evolved massive stars. Their idea relies on the fact that the surface nitrogen content of massive stars reaches a maximum during evolution due to production of N through the CNO cycle. Observationally, this maximum is obtained in WN stars. Its exact value is independent of the initial mass and of the wind properties. It changes with the initial metal content since the amount of Nitrogen synthesized is directly linked to the initial CNO content. Hence, the comparison of derived N abundances in WN stars to evolutionary tracks is an indirect tracer of the initial metallicity.

In Table 2 we list our derived nitrogen mass fraction. Only for WN stars such an estimate could be performed due to the presence of N III lines in the K band spectrum, especially N III 2.247, 2.251 μm. For most stars, we have $X(N) \approx 0.0135$, with the exception of IRS15SW and AFNW which show a larger N content (up to 0.0326). However, for the latter star the uncertainty on the N abundance determination is quite large due to the low resolution and low S/N ratio of our spectrum. A direct comparison of this range of values to predictions of surface enrichment in evolutionary models (see e.g. Fig. 4 of Najarro et al. 2004) indicates an initial metallicity between solar and twice solar. If IRS15SW and AFNW are not taken into account, then a solar metallicity is favoured. Strictly speaking, we derive a lower limit since one cannot be sure that all WN stars have reached the phase in which their surface N abundance is maximum. Indeed, although this phase is long for initially very massive stars, it is quite short for stars with $M \sim 20$–$50\ M_\odot$ which is more appropriate for our WN8 stars. In conclusion, we estimate the stellar GC metallicity to be *at least* solar. Stronger constraints cannot be derived from the present set of data/models.

Stellar studies usually indicate a solar metallicity for the GC. Najarro et al. (2004) found $Z = Z_\odot$ for WN stars in the Arches cluster. This is also comparable to the determinations of Carr et al. (2000) and Ramírez et al. (2000) who also derived a solar [Fe/H] from the study of iron lines in red supergiants in the central 2.5 pc.

Abundances have also been derived from interstellar gas studies. Shields & Ferland (1994) derived solar Ne content and twice solar Ar and N based on photoionisation models aimed at reproducing nebular fine structure lines in the mid infrared. However, improvements in the knowledge of the Ar collisional strengths led to a revision of the Ar abundance down to a nearly solar value (see discussion in Carr et al. 2000). This is to be contrasted by the recent analysis of ISO data by Giveon et al. (2002) who found Ne ~ 1.4 Ne$_\odot$ and Ar ~ 2.5 Ar$_\odot$. Similarly, Martín-Hernández et al. (2003) revised the Galactic metallicity gradients. Extrapolating their results to the Galactic Center, one should expect n(Ne/H) $\sim$ n(Ar/H) $\sim$ 1.5−2.5 $Z_\odot$ and n(N/H) $\sim 5\ Z_\odot$.

Finally, observations of K shell Fe lines by Chandra have been used by Maeda et al. (2002) to derive an iron content as large as 4 times solar for the H II region SgrA East. Such a large metallicity was recently confirmed on a larger scale by X-ray observations with Suzaku (Koyama 2006).

Clearly, the measurement of the metallicity in the Galactic Center needs more investigation. We have seen in Sects. 4.1.3 and 4.2.1 that individual elemental abundances could be super-solar (Mg, Si). But the uncertainties associated to these estimates did not allow a reliable statement. The use of high signal to noise, high spectral resolution data is mandatory in order to resolve weak metallic lines of Ofpe/WN9 stars, red supergiants as well as AGB stars. The distinction between α element and Iron abundances is also crucial. α elements are essentially produced in massive stars while Iron is mainly synthesized in low mass stars during the type Ia supernova phase. The ratio of α elements to Iron abundances is thus an indirect tracer of the slope of the IMF.

7.2. Metallicity effect on HeI 2.058 μm

We have seen in Sect. 4.2.3 that He I 2.058 μm is extremely sensitive to the metal content. Indeed, the higher the metallicity, the stronger the line emission so that $Z = 2 \times Z_\odot$ was actually preferred for IRS9W. Such a behavior was previously noted by Crowther et al. (1998) and Bohannan & Crowther (1999) and was attributed to the sensitivity of He I 2.058 μm to the EUV radiation field, which in turn depends critically on the heavy-metal content. Figure 24 shows the He ionisation and temperature structure of the models for IRS9W with $Z = Z_\odot$ and $Z = 2 \times Z_\odot$. This figure helps us understand in detail what happens when the metal content is increased. Due to the larger blocking of radiation by metal opacities, the EUV flux is reduced which reduces the ionisation in the outer part of the atmosphere (see lower panel of Fig. 24). In addition, the escape of radiation through metallic lines is favored so that the efficiency of line cooling is enhanced, leading to a reduction of the temperature for $\log \tau_{\rm Rosseland} \leq -1.0$ (upper panel of Fig. 24). Both effects (line cooling and line blocking) increase the He I content in the outer atmosphere. In Fig. 24, we also indicate the line formation region of He I 2.058 μm and He II 2.189 μm. We see that He II 2.189 μm emerges from a zone where the atmospheric structure is barely modified, so that its strength is similar in both models (see Fig. 9). On the other hand, He I 2.058 μm is produced in the outer atmosphere where the amount of He I is larger in the $Z = 2 \times Z_\odot$ model. Consequently, He I 2.058 μm is stronger in the high metallicity model. Note that this explanation is fully consistent with the approach of Najarro et al. (1994): when metallicity is increased, the He I content increases which leads to a decrease of the escape probability of the He I 584 Å line controlling the upper level of He I 2.058 μm – He II being the dominant ionisation state. This implies a stronger emission at 2.058 μm(see Eq. (2) of Najarro et al. 1994).

Does that mean that a twice solar metallicity should be adopted for IRS9W? This would be an over-interpretation of the results. Indeed, what the previous exercise reveals is that He I 2.058 μm is extremely sensitive to the EUV radiation. We cannot be absolutely sure that we correctly predict this part of the spectrum. Indeed, our models are limited in the sense that we cannot include *all* lines from *all* elements. He I 2.058 μm may also suffer from inaccuracies in metal atomic data. Hence, it may well be that increasing the metal content artificially compensates for the lack of metallic lines / elements. Besides, we have discussed only one example for which a larger metal content improves the fit of He I 2.058 μm. But there are other stars (e.g. IRS7E2) for which having a higher Z does not help, He I 2.058 μm remaining too weak. Hence, we conclude that the metallicity cannot be accurately derived from its effect on He I 2.058 μm.

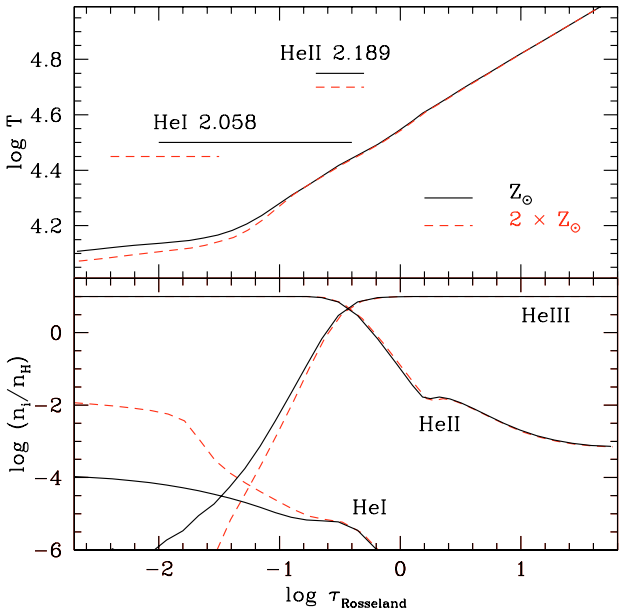

Fig. 24. Temperature (*upper panel*) and He ionisation (*lower panel*) structure of the best fit model for IRS9W. The solid line is the model with solar metallicity, while the dashed line is for $Z = 2 \times Z_\odot$. In the upper panel, the line formation regions of He I 2.058 μm and He II 2.189 μm are indicated by horizontal lines.

8. Wind properties of Wolf-Rayet stars

We have derived the wind properties of a homogeneous and reasonably large sample of Wolf-Rayet stars, mainly composed of WN and Ofpe/WN9 stars. In order to see if the GC stellar winds are similar to other Galactic WR stars, we inspect the behavior of the terminal velocities and mass loss rates (corrected for clumping).

Terminal velocities for other Galactic stars are taken from the catalog of van der Hucht (2001) and are compared to our sample in Fig. 25. We see that there is a remarkable agreement. We have seen in Sect. 6.1 that v_∞ is usually larger in the GC than in the LMC for Ofpe/WN9 stars, but this was at least qualitatively explained by a different metallicity/evolutionary state. We then conclude that the terminal velocities of the GC Wolf-Rayet stars are identical to other Galactic stars.

The mass loss rates of WN and Ofpe/WN9 stars are shown in Fig. 26 as a function of luminosity[5]. We also plot the results of Crowther et al. (1995c), Crowther et al. (1995b), Morris et al. (2000), (all in blue open symbols) and Hamann et al. (2006) (black filled symbols). The GC mass loss rates are in good agreement with the Crowther et al./Morris et al. results for late WN stars (triangles). For early WN stars, the samples are too small to draw any conclusion. On the contrary, there is a large discrepancy between our results and those of Hamann et al. (2006), at least for late WN stars. This difference is not so much due to the mass loss rates themselves as it is to luminosities. Indeed, both samples have similar values of $\dot{M}/\sqrt{f}$, but the luminosities in the GC are lower. Since most of the stars of the Hamann et al. sample have poorly constrained distances (only

[5] Our sample of WC stars is too small for a comparison to other Galactic stars to be relevant.

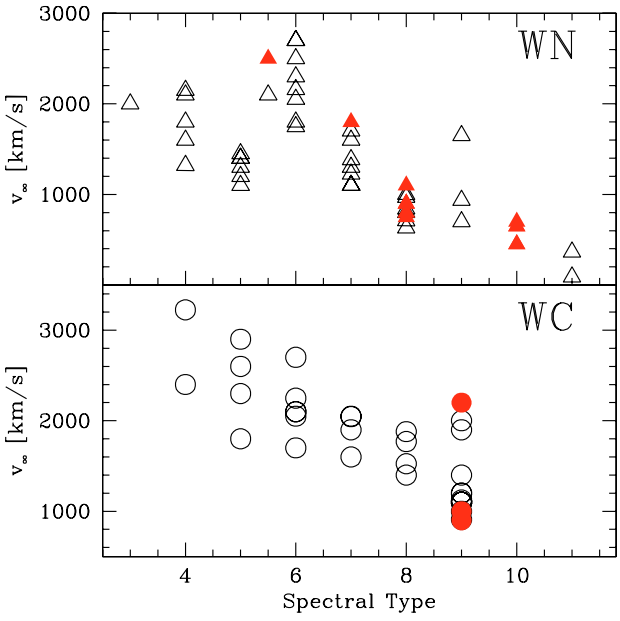

Fig. 25. Terminal velocity of GC WR stars (filled symbols) and other Galactic stars (open symbols) as a function of spectral type. The data for galactic stars are taken from the compilation of van der Hucht (2001). *Upper panel*: WN stars; *Lower panel*: WC stars.

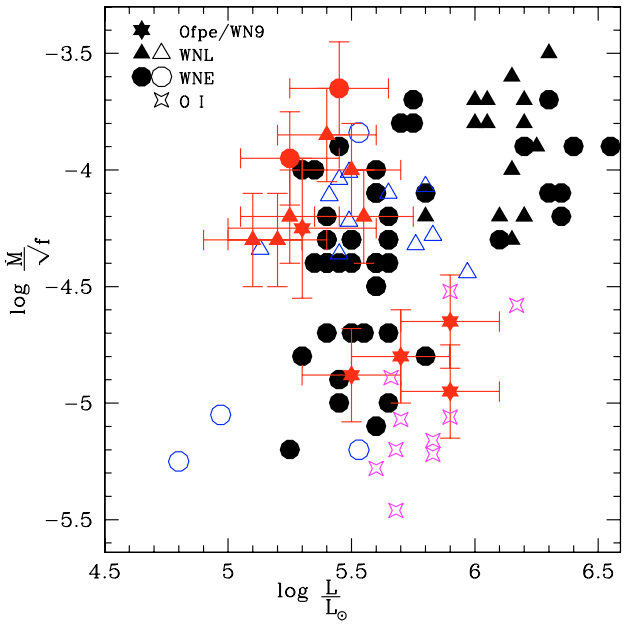

Fig. 26. Mass loss rate corrected for clumping ($\dot{M}/\sqrt{f}$) as a function of luminosity for GC WN stars (red filled symbols) compared to other Galactic Wolf-Rayet stars (blue and black symbols) and O supergiants (magenta star symbols). Comparison data from Crowther et al. (1995b), Crowther et al. (1995c), Morris et al. (2000) for WN stars and Repolust et al. (2004), Bouret et al. (2005) for O supergiants are shown by open symbols. The results of Hamann et al. (2006) (WN stars) are displayed by the black filled symbols. Early WN stars (≤WN7) are shown by triangles, while late WN stars (≥WN8) are circles. Ofpe/WN9 stars are star symbols and O supergiants are open asterisks.

a few are in clusters), while the distance to the GC is accurately known, we argue that the main reason for the observed difference is an overestimate of the luminosities in the Hamann et al. sample. An additional explanation to the GC/Hamann et al. WNL luminosity difference could be that their sample contains several H-rich WN stars. These stars are thought to be very massive stars with a Wolf-Rayet appearance but possibly still core H burning objects on/close to the main sequence (e.g. Moffat et al. 2006). Such stars are expected to be very luminous. However, they usually have spectral subtypes earlier than WN7 (e.g. Crowther & Dessart 1998). A significant fraction of the very luminous stars in the Hamann et al. sample (represented by filled triangles around $\log \frac{L}{L_\odot} \sim 6.0$–$6.2$ in Fig. 26) do not fall into this category (they are later WN stars). Their luminosity is thus most likely overestimated due to poorly known distance.

In Fig. 26, we also plot the mass loss rates of the GC Ofpe/WN9 stars together with Galactic O supergiants. We see that in terms of $\dot{M}$, the Ofpe/WN9 stars are closer to O stars than to WN stars. This is another indication that Ofpe/WN9 stars are precursors of WN8 stars as we have argued in Sect. 6.2.

9. He abundance in OB stars

We have seen in Sect. 4.4 that the stellar and wind parameters of the average OB stars in the central parsec were not strongly constrained. Most of them have only upper limits ($T_{\rm eff}$, $\dot{M}$). For the helium content, we could estimate X(He) $\simeq$ 0.2–0.35. This value is larger than the standard solar abundance (0.1).

Since OB supergiants are massive stars evolving away from the main sequence, chemical enrichment is the most likely explanation. The question is whether or not the amount of He observed is consistent with such a mechanism. In that respect, the inclusion of rotation in evolutionary models is a key ingredient since it triggers additional mixing which modifies the He surface abundance X(He). In the recent models of Meynet & Maeder (2005), X(He) evolves slowly from the initial value during all the "O" phase, and then dramatically increases when the star enters the Wolf-Rayet phase. At the end of the O phase, a He content as large as 0.3–0.4 can be obtained. This is compatible with our derived value. We have also seen in Sect. 4.4 that the average projected rotational velocity of the brightest OB supergiants was of the order 100 km s^{-1}. Inspection of Fig. 1 of Meynet & Maeder (2003) reveals that after 4–8 Myr (age of the GC population of early type stars), stars with initial masses in the range 25–60 $M_\odot$ (appropriate for the OB supergiants) have indeed $V \sin i$ between 40 and 200 km s^{-1} (depending on the exact age / mass). This is another indication that 1) the evolutionary tracks with rotation are adequate for the present discussion, and 2) that the GC massive stars do not have exceptionally large rotational velocities, as could be suspected for such a dense environment where interactions should be frequent.

How does our He determination compare to other analyses of massive stars? The answer is given in Fig. 27. Blue circles show the He content of Galactic O supergiants. It is important to note that the uncertainty usually quoted in such determinations is ±0.05–0.1. The circle with the error bars in Fig. 27 represents the average OB supergiants in the GC. We see that although large, the He content of these stars is still compatible with the range of values found for O supergiants. In conclusion, the GC OB supergiants are *on average* similar to other Galactic stars in terms of He enrichment. This abundance is in addition compatible with present evolutionary tracks.

Paumard et al. (2006) noted that a few OB supergiants had a strong He absorption on the blue side of Br$_\gamma$ and suggested that these stars are significantly He-rich. Unfortunately, given the low S/N ratio spectra of these stars, we could not derive quantitative constraints on the He abundance.

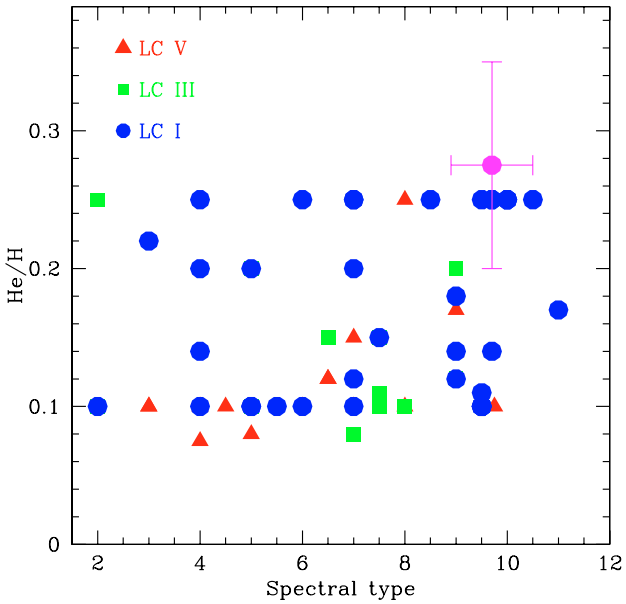

Fig. 27. Comparison between derived ratio of He to H abundance (symbol with error bars) of OB supergiants in the Galactic Center to values from other studies (Herrero et al. 2001; Bouret et al. 2003; Evans et al. 2004; Markova et al. 2004; Repolust et al. 2004). Red triangles (green squares; blue circles) are dwarfs (giants; supergiants).

10. Conclusion

We have carried out a detailed analysis of 18 evolved massive stars (Ofpe/WN9 and Wolf-Rayet) located in the central parsec of the Galaxy from *H* and *K* band spectroscopy obtained with SINFONI on the ESO/VLT. The average spectrum of 10 bright OB supergiants was also examined. For quantitative analysis, we have used state of the art non-LTE atmosphere models including winds and line-blanketing computed with the code CMFGEN. The main results are:

- The population of massive stars in the central parsec is able to supply the amount of H and HeI ionising photons required to reproduce the nebular emission. The contribution of the bright, cool post-main sequence massive stars, first discovered by Forrest et al. (1987) and Allen et al. (1990) and analysed by Najarro et al. (1997), accounts for only ∼4% of the total H ionising flux reconciling stellar evolution with observations in the Galactic Center. State of the art evolutionary and atmosphere models also reconcile the observed stellar content with a population synthesis model of a starburst of age ∼6 Myr.
- Ofpe/WN9 stars are evolved massive stars close to a LBV phase. Compared to Najarro et al. (1997), we find they are less He rich, slightly hotter (although the temperature is poorly constrained) and have lower mass loss rates. WN8 stars are found to have properties similar to other Galactic Wolf-Rayet stars of the same spectral type. From morphological as well as quantitative arguments, they are likely the descendents of Ofpe/WN9 stars. Two stars are classified as WN8/WC9 stars. Their quantitative analysis reveals that, as suggested by their spectral type, they show both H and He burning products at their surface. A direct evolutionary link between the GC Ofpe/WN9, WN8 and WN/C stars of the form

  (Ofpe/WN9 $\rightleftharpoons$ LBV) $\rightarrow$ WN8 $\rightarrow$ WN/C

  is proposed, similar to Crowther et al. (1995b).
- Quantitatively, stellar evolutionary tracks with rotation and $Z = Z_{\odot}$ overpredict the luminosity of the GC Wolf-Rayet stars. Tracks with $Z = 2 \times Z_{\odot}$ are more appropriate. This may indicate that the mass loss rates adopted in the current evolutionary tracks during the Wolf-Rayet phase are too low. However, accurate metallicity determinations are needed to solve this issue.
- On average, GC OB supergiants are He rich, but not significantly richer than other galactic supergiants. Their present projected rotational velocities is ∼100 km s^{-1}. These properties are quantitatively compatible with stellar evolution with rotation on and close to the main sequence.
- The wind properties of WN stars in the Galactic center are very similar to other Galactic stars of the same spectral type. The luminosities of late WN stars are lower in the GC than in the sample of Hamann et al. (2006) but in good agreement with the results of Crowther et al. (1995b). We argue that the difference with the results of Hamann et al. is due to uncertain distances for their sample stars, while in our case the distance to the GC is well constrained.

Our study has shown that the GC massive stars are, on average, similar to other Galactic stars. This strongly suggests that they follow a common evolution, regardless of their possible different formation process. A key question which remains to be addressed in future studies is the metallicity in the GC. A better knowledge of this parameter is crucial to quantitatively test evolutionary models. It is also crucial in the context of the chemical evolution of the Galaxy. Also important is the study of nebular emission in the GC by means of recently developed 3D photoionization models. Our total stellar SED will be a crucial input for such models which will likely constrain the geometry and density of the ionised gas.

Acknowledgements. We thank F. Najarro for interesting discussions. F.M. acknowledges support from the Alexander von Humboldt foundation.

References

Allen, D. A., Hyland, A. R., & Hillier, D. J. 1990, MNRAS, 244, 706
Anderson, L. 1991, in Stellar Atmospheres – Beyond Classical Models, NATO ASIC Proc., 341, 29
Antokhin, I., Bertrand, J.-F., Lamontagne, R., Moffat, A. F. J., & Matthews, J. 1995, AJ, 109, 817
Bohannan, B., & Crowther, P. A. 1999, ApJ, 511, 374
Bonnet, H., Abuter, R., Baker, A., et al. 2004, The Messenger, 117, 17
Bouret, J.-C., Lanz, T., Hillier, D. J., et al. 2003, ApJ, 595, 1182
Bouret, J.-C., Lanz, T., & Hillier, D. J. 2005, A&A, 438, 301
Bresolin, F., Kudritzki, R.-P., Najarro, F., Gieren, W., & Pietrzyński, G. 2002, ApJ, 577, L107
Carr, J. S., Sellgren, K., & Balachandran, S. C. 2000, ApJ, 530, 307
Clénet, Y., Rouan, D., Gendron, E., et al. 2004, A&A, 417, L15
Crowther, P. A., Bohannan, B., & Pasquali, A. 1998, in Properties of Hot Luminous Stars, ed. I. Howarth, ASP Conf. Ser., 131, 38
Crowther, P. A., & Dessart, L. 1998, MNRAS, 296, 622
Crowther, P. A., & Smith, L. J. 1996, A&A, 305, 541
Crowther, P. A., & Smith, L. J. 1997, A&A, 320, 500
Crowther, P. A., Hillier, D. J., & Smith, L. J. 1995a, A&A, 293, 172
Crowther, P. A., Hillier, D. J., & Smith, L. J. 1995b, A&A, 293, 403
Crowther, P. A., Smith, L. J., & Hillier, D. J. 1995c, A&A, 302, 457
Crowther, P. A., Smith, L. J., & Willis, A. J. 1995d, A&A, 304, 269
Crowther, P. A., Hillier, D. J., Evans, C. J., et al. 2002, ApJ, 579, 774
Crowther, P. A., Morris, P., & Smith, J. D. 2006, ApJ, in press
Eisenhauer, F., Abuter, R., Bickert, K., et al. 2003a, in Instrument Design and Performance for Optical/Infrared Ground-based Telescopes, ed. I. Masanori, A. F. M. Moorwood, Proc. SPIE, 4841, 1548
Eisenhauer, F., Tecza, M., Thatte, N., et al. 2003b, The Messenger, 113, 17
Eisenhauer, F., Genzel, R., Alexander, T., et al. 2005, ApJ, 628, 246
Ekers, R. D., van Gorkom, J. H., Schwarz, U. J., & Goss, W. M. 1983, A&A, 122, 143

Evans, C. J., Crowther, P. A., Fullerton, A. W., & Hillier, D. J. 2004, ApJ, 610, 1021
Ferland, G. J., Korista, K. T., Verner, D. A., et al. 1998, PASP, 110, 761
Figer, D. F., McLean, I. S., & Najarro, F. 1997, ApJ, 486, 420
Figer, D. F., McLean, I. S., & Morris, M. 1999, ApJ, 514, 202
Figer, D. F., Najarro, F., Gilmore, D., et al. 2002, ApJ, 581, 258
Forrest, W. J., Shure, M. A., Pipher, J. L., & Woodward, C. E. 1987, in The Galactic Center, ed. D. C. Backer, AIP Conf. Proc., 155, 153
Fullerton, A. W., Massa, D. L., & Prinja, R. K. 2006, ApJ, 637, 1025
Geballe, T. R., Najarro, F., Rigaut, F., & Roy, J.-R. 2006, ApJ
Genzel, R., Watson, D. M., Townes, C. H., et al. 1984, ApJ, 276, 551
Genzel, R., Crawford, M. K., Townes, C. H., & Watson, D. M. 1985, ApJ, 297, 766
Genzel, R., Hollenbach, D., & Townes, C. H. 1994, Rep. Progr. Phys., 57, 417
Genzel, R., Schödel, R., Ott, T., et al. 2003, ApJ, 594, 812
Gerhard, O. 2001, ApJ, 546, L39
Ghez, A. M., Duchêne, G., Matthews, K., et al. 2003, ApJ, 586, L127
Giveon, U., Morisset, C., & Sternberg, A. 2002, A&A, 392, 501
Grevesse, N., & Sauval, A. J. 1998, Space Sci. Rev., 85, 161
Hamann, W., Gräfener, G., & Liermann, A. 2006, A&A, 457, 1015
Heger, A., & Langer, N. 1996, A&A, 315, 421
Herald, J. E., Hillier, D. J., & Schulte-Ladbeck, R. E. 2001, ApJ, 548, 932
Herrero, A., Puls, J., Corral, L. J., Kudritzki, R. P., & Villamariz, M. R. 2001, A&A, 366, 623
Hillier, D. J., & Miller, D. L. 1998, ApJ, 496, 407
Hillier, D. J., Lanz, T., Heap, S. R., et al. 2003, ApJ, 588, 1039
Horrobin, M., Eisenhauer, F., Tecza, M., et al. 2004, Astron. Nachr., 325, 88
Hubeny, I., & Lanz, T. 1995, ApJ, 439, 875
Kim, S. S., & Morris, M. 2003, ApJ, 597, 312
Koyama, K. E. A. 2006, PASJ, in press
Krabbe, A., Genzel, R., Drapatz, S., & Rotaciuc, V. 1991, ApJ, 382, L19
Krabbe, A., Genzel, R., Eckart, A., et al. 1995, ApJ, 447, L95
Lamers, H. J. G. L. M., & Cassinelli, J. P. 1999, Introduction to Stellar Winds (Introduction to Stellar Winds, ed. Henny J. G. L. M. Lamers, & Joseph P. Cassinelli (Cambridge, UK: Cambridge University Press), 452
Langer, N. 1991, A&A, 248, 531
Lenorzer, A., Mokiem, M. R., de Koter, A., & Puls, J. 2004, A&A, 422, 275
Levin, Y., & Beloborodov, A. M. 2003, ApJ, 590, L33
Lutz, D. 1999, in The Universe as Seen by ISO, ed. P. Cox, & M. Kessler, ESA SP-427, 623
Maeda, Y., Baganoff, F. K., Feigelson, E. D., et al. 2002, ApJ, 570, 671
Maeder, A., & Meynet, G. 2000, ARA&A, 38, 143
Maillard, J. P., Paumard, T., Stolovy, S. R., & Rigaut, F. 2004, A&A, 423, 155
Marchenko, S. V., Moffat, A. F. J., Eversberg, T., et al. 1998, MNRAS, 294, 642
Markova, N., Puls, J., Repolust, T., & Markov, H. 2004, A&A, 413, 693
Martín-Hernández, N. L., van der Hulst, J. M., & Tielens, A. G. G. M. 2003, A&A, 407, 957
Martins, F., Schaerer, D., & Hillier, D. J. 2002, A&A, 382, 999
Martins, F., Schaerer, D., & Hillier, D. J. 2005, A&A, 436, 1049
Martins, F., Schaerer, D., Hillier, D. J., & Heydari-Malayeri, M. 2004, A&A, 420, 1087
Martins, F., Trippe, S., Paumard, T., et al. 2006, ApJ, 649, L103
Massey, P., & Grove, K. 1989, ApJ, 344, 870
Meynet, G., & Maeder, A. 2003, A&A, 404, 975
Meynet, G., & Maeder, A. 2005, A&A, 429, 581
Moffat, A. F. J., Schnurr, O., Chené, A.-N., St-Louis, N., & Casoli, J. 2006, Calibrating the Top of the Stellar M-L Relation, 26th meeting of the IAU, Joint Discussion 5, 16 August 2006, Prague, Czech Republic, JD05, #1, 5
Morisset, C., Schaerer, D., Bouret, J.-C., & Martins, F. 2004, A&A, 415, 577
Morris, M. 1993, ApJ, 408, 496
Morris, P. W., van der Hucht, K. A., Crowther, P. A., et al. 2000, A&A, 353, 624
Moultaka, J., Eckart, A., Schödel, R., Viehmann, T., & Najarro, F. 2005, A&A, 443, 163
Najarro, F., Hillier, D. J., Kudritzki, R. P., et al. 1994, A&A, 285, 573
Najarro, F., Figer, D. F., Hillier, D. J., & Kudritzki, R. P. 2004, ApJ, 611, L105
Najarro, F., Hillier, D. J., Puls, J., Lanz, T., & Martins, F. 2006, A&A, 456, 659
Najarro, F., Krabbe, A., Genzel, R., et al. 1997, A&A, 325, 700
Nayakshin, S., & Cuadra, J. 2005, A&A, 437, 437
Pasquali, A., Langer, N., Schmutz, W., et al. 1997, ApJ, 478, 340
Paumard, T., Maillard, J. P., Morris, M., & Rigaut, F. 2001, A&A, 366, 466
Paumard, T., Genzel, R., Maillard, J. P., et al. 2004, in Young Local Universe, Proceedings of XXXIXth Rencontres de Moriond, La Thuile, Aosta Valley, Italie, March 21–28, 2004, ed. A. Chalabaev, T. Fukui, T. Montmerle, & J. Tran-Thanh-Van (Paris: Éditions Frontieres), 377
Paumard, T., Genzel, R., Martins, F., et al. 2006, ApJ, 643, 1011
Puls, J., Kudritzki, R.-P., Herrero, A., et al. 1996, A&A, 305, 171
Ramírez, S. V., Sellgren, K., Carr, J. S., et al. 2000, ApJ, 537, 205
Repolust, T., Puls, J., & Herrero, A. 2004, A&A, 415, 349
Repolust, T., Puls, J., Hanson, M. M., Kudritzki, R.-P., & Mokiem, M. R. 2005, A&A, 440, 261
Schaerer, D. 1996, in ASP Conf. Ser.: AGN, Dense Stellar Systems, and Galactic Environments, ed. S. Lamb, & J. Perry
Schoedel, R., et al. 2007, A&A
Shields, J. C., & Ferland, G. J. 1994, ApJ, 430, 236
Smith, L. J., Norris, R. P. F., & Crowther, P. A. 2002, MNRAS, 337, 1309
Stolte, A., Grebel, E. K., Brandner, W., & Figer, D. F. 2002, A&A, 394, 459
Thornley, M. D., Schreiber, N. M. F., Lutz, D., et al. 2000, ApJ, 539, 641
Trippe, S., Martins, F., Ott, T., et al. 2006, A&A, 448, 305
Tuthill, P. G., Monnier, J. D., & Danchi, W. C. 1999, Nature, 398, 487
Tuthill, P., Monnier, J., Tanner, A., et al. 2006, Science, in press
van der Hucht, K. A. 2001, VizieR Online Data Catalog, 3215, 0
Williams, P. M., van der Hucht, K. A., & The, P. S. 1987, A&A, 182, 91
Willis, A. J., & Stickland, D. J. 1990, A&A, 232, 89